In-situ observation of mitochondrial biogenesis as the early event of apoptosis

Chang-Sheng Shao [1,2], Xiu-Hong Zhou [3], Yu-Hui Miao [4], Peng Wang[1], Qian-Qian Zhang [1,2] and Qing Huang [1,2] *

[1] CAS Key Laboratory of High Magnetic Field and Ion Beam Physical Biology, Hefei Institutes of Physical Science, Chinese Academy of Sciences (CAS), Hefei 230031, China;

[2] Science Island Branch of Graduate School, University of Science and Technology of China, Hefei 230026, China;

[3] Center of Biology, Anhui Agricultural University, Hefei, China;

[4] Department of Medical Oncology, The First Affiliated Hospital of USTC, Division of Life Sciences and Medicine, University of Science and Technology of China, Hefei, China;

***Corresponding author:**

Prof. Qing Huang

Hefei Institutes of Physical Science, Chinese Academy of Sciences, P. O. Box 1138, Hefei 230031, P.R. China

Tel: 86-551-65595261; Fax: 86-551-65595261

E-mail: huangq@ipp.ac.cn

Abstract

Mitochondrial biogenesis is a cell response to external stimuli which is generally believed to suppress apoptosis. However, during the process of apoptosis, whether mitochondrial biogenesis occurs in the early stage of the apoptotic cells remains unclear. To address this question, we constructed the COX8-EGFP-ACTIN-mCherry HeLa cells with recombinant fluorescent proteins respectively tagged on the nucleus and mitochondria, and monitored the mitochondrial changes in living cells exposed to gamma-ray radiation. Besides in situ detection of mitochondrial fluorescence changes, we also examined the cell viability, nuclear DNA damage, reactive oxygen species (ROS), mitochondrial DNA copy number and expression of transcription genes related to mitochondrial biogenesis as well as the apoptosis biomarkers. As a result, we confirmed that significant mitochondrial biogenesis took place preceding the radiation-induced apoptosis, and the change of mitochondrial biogenesis at early time was closely correlated with the apoptotic cells at late stage. The involved mechanism was also discussed.

Keywords: mitochondrial biogenesis; apoptosis; fluorescent proteins; ionizing radiation; living cells; DNA damage

Abbreviations: AICAR, 5-Aminoimidazole-4-carboxamide ribotide; ANOVA, Analysis of Variance; CCK-8, Cell Counting Kit-8; CytoC, Cytochrome C; DMEM, Dulbecco's modified Eagle's medium; DSB, Double strand breakage; *E. coli, Escherichia coli*; HCS, High-content screening; H2DCFDA, 2',7'-

44 dichlorodihydrofluorescein diacetate; HR, Homologous recombination mediated repair;
45 LDH, Lactate Dehydrogenase; MMP, Mitochondrial membrane potential; MFI, mean
46 fluorescence intensity; Mfn1, Mitofusin 1; mtDNA, Mitochondrial DNA; nDNA,
47 nuclear DNA; NHEJ, Non homologous end joining; PI, Propidium iodide; PARP, Poly
48 ADP-Ribose Polymerase; PGC-1α, Peroxisome proliferator-activated receptor-gamma
49 coactivator (PGC)-1alpha; RT-qPCR, Real-Time Quantitative Reverse Transcription
50 PCR; ROS, reactive oxygen species; SD, standard derivation; SIRT, Silent information
51 regulator; TMRE, Tetramethylrhodamine ethyl ester; TFAM, transcription factor A,
52 mitochondrial.
53

Synopsis

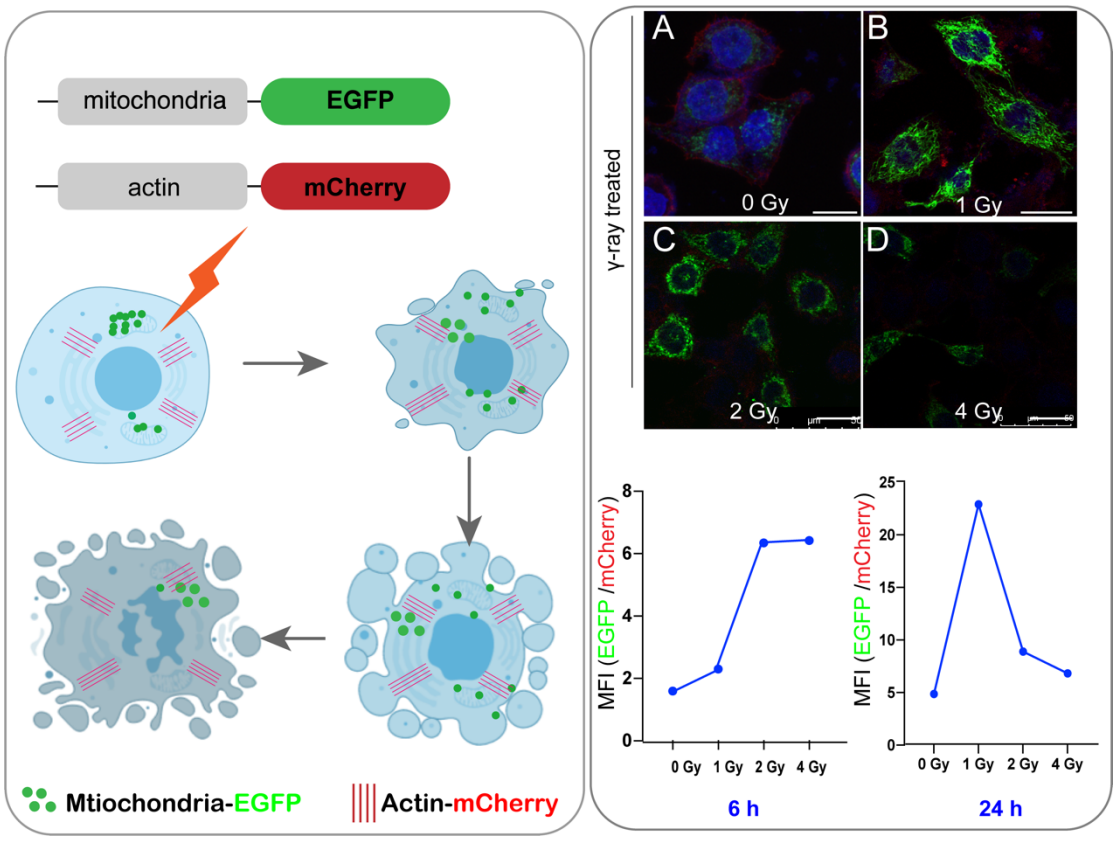

This study revealed that significant mitochondrial biogenesis could take place even when the cells were destined to the fate of apoptosis, and therefore for the first time explicitly demonstrated that mitochondrial biogenesis could be positively correlated with apoptosis given that these events were evaluated at right separate time points with consideration of their logical time-sequence of occurrence.

Highlights

- A dual fluorescence reporter system was constructed for in-situ observation of mitochondrial biogenesis in living cells.
- Significant mitochondrial biogenesis in the radiation-induced apoptosis was observed.
- Positive correlation of early mitochondrial biogenesis with late apoptosis was

68 explicitly revealed.

69 - Assessment of the early event of mitochondrial biogenesis is critical for prediction
70 of the late fate of cells.

71 ## Introduction

72 Mitochondrial biogenesis is a physiological response of cells to external stress and
73 development signals that may cause increase of energy demand, and it plays an
74 important role in cell metabolism regulation, signal transduction and mitochondrial
75 ROS regulation (Luo *et al*, 2016; Vyas *et al*, 2016). Mitochondrial biogenesis maintains cell
76 homeostasis by ensuring the quality of mtDNA and regulating the renewal of organelles
77 (Yambire *et al*, 2019), and it has been extensively explored in recent years due to its related
78 interests in human aging, neurodegenerative diseases, cell metabolic diseases and
79 tumors(Fanibunda *et al*, 2019).

80 Since mitochondrial regulation plays a very critical role in controlling the cell fate,
81 it is also intriguing for researchers to explore the relationship between mitochondrial
82 biogenesis and apoptosis. Generally, apoptosis is mediated by the activation of the
83 caspase pathways which are accompanied with mitochondrial damage accompanied by
84 destruction of electron transfer, oxidative phosphorylation, ATP production and change
85 of cell redox potential(Burke, 2017). In fact, some studies have claimed that there is a
86 negative correlation between mitochondrial biogenesis and apoptosis, i.e., apoptosis
87 may be substantially suppressed by mitochondrial biogenesis. For example, it has been
88 reported that stress-induced apoptosis can be inhibited by enhanced mitochondrial
89 biogenesis (Dam *et al*, 2013), or, on the other hand, apoptosis and cell cycle arrest may
90 occur by inhibiting mitochondrial biogenesis(Cao *et al*, 2017). Also, in the study of

91 radiation-induced apoptosis, mitochondrial biogenesis was observed and analyzed (Rai
92 *et al*, 2018), and it was claimed that enhancement of mitochondrial biogenesis could
93 reduce the proportion of apoptosis caused by ionizing radiation(Yu *et al*, 2013). However,
94 regarding the whole process of apoptosis, whether and how mitochondrial biogenesis
95 takes place in the early period in the apoptotic cells exposed to the external stimuli such
96 as ionizing radiation remains elusive.

97 To study the process of mitochondrial biogenesis related to apoptosis, it is thus
98 crucial to monitor the mitochondrial changes in the cells. At present, there are not many
99 methods available to study the influence of external factors on mitochondrial changes.
100 One of the conventional methods is to probe the change of mitochondrial gene copy
101 numbers(Yu, 2011). Another approach is to use fluorescent proteins. Fluorescent proteins
102 are beneficial for studying the living cells with reporting gene expression, which can
103 provide information on protein locations and expression levels as well as the involved
104 biochemical activities(Newman *et al*, 2011). Actually, study of mitochondrial process
105 using fluorescent proteins is now attracting increasing attention (Melentijevic *et al*, 2017;
106 Katajisto *et al*, 2015; Ruan *et al*, 2017). Recent development is to make use of multiple
107 different fluorescent proteins with different excitation/emission spectra, so that the
108 precision of transcriptional measurements can be ensured by using the reference color
109 for normalization (Miyashiro & Goulian, 2007). In such a circumstance, the ratio of dual
110 fluorescence can be used to eliminate the possible fluorescence measurement
111 errors(Miyashiro & Goulian, 2007). So, with application of this dual fluorescence approach,
112 nowadays researchers are able to observe and analyze the temporal and spatial life

113 trajectories of living cells (Jadhav & Shivdasani, 2019), and maybe more importantly, to
114 scrutinize the early events leading to various bio-effects such as apoptosis as end-point
115 fate in the living cells (Yu *et al*, 2020).

116 Therefore, in the present work, we attempted to apply the dual recombinant
117 fluorescent proteins to monitor the mitochondrial biogenesis induced by radiation, and
118 in this way, to examine whether and how the early event of mitochondrial biogenesis
119 would be associated with the prominent bio-effect such as apoptosis. For the effect of
120 radiation as the external stimuli to the cells, it is known that ionizing radiation (such as
121 α-, γ-, X-rays, protons, heavy ions) can readily cause various detrimental damages to
122 living cells, which can lead to the change of genetic information, cell mutations,
123 genomic instability, and apoptosis (O'Driscoll & Jeggo, 2006). Mitochondria, as important
124 subcellular organelles, are one of the major targets of ionizing radiation as they occupy
125 a considerable proportion of the cell volume (4-25%)(Leach *et al*, 2001). On the other
126 hand, radiation can also effectively induce mitochondrial biogenesis (Das *et al*, 2020). For
127 the establishment of the dual fluorescent system for in-situ observation of
128 mitochondrial biogenesis in living cells, we constructed the stable fluorescent reporter
129 cell lines by lentiviral transfection to achieve mitoGFP and nuclear RFP. As a result, we
130 fulfilled the task of in-situ and real-time observation of mitochondrial changes in the
131 living cells, and observed the effect of mitochondrial biogenesis occurring in the early
132 process of the apoptotic cells. By analyzing the fluorescence ratio of mitoGFP and
133 nuclear mCherry fluorescence, we could therefore examine the relationship between
134 the early mitochondrial biogenesis and late apoptosis, and testified that the increased

135 mitochondria number in the early time could be positively correlated with the apoptotic
136 cell population. The detailed mitochondrial/apoptotic processes were analyzed, and the
137 involved mechanism was discussed.

138 # Results

139 ## Construction of dual-fluorescent stably transfected cell lines

140 In order to construct a universal dual-fluorescence gene reporter vector, we
141 considered to make use of the simplicity of vector construction and referred to the
142 previously reported dual-fluorescence reporter system, and so we chose the CMV
143 promoter to express the dual-fluorescence target proteins. The mitochondrial reporter
144 expression system is generally localized in the stroma, targeting the leader peptide
145 (MSVLTPLLLRGLTGSARRLPVPRAKIHSLGDP) on the VIIIa subunit of
146 cytochrome C (COX8) (Haggie & Verkman, 2002) (Fig 1A). As such, we constructed the
147 pLVX-mCherry-actin lentiviral vector (Fig 1B).

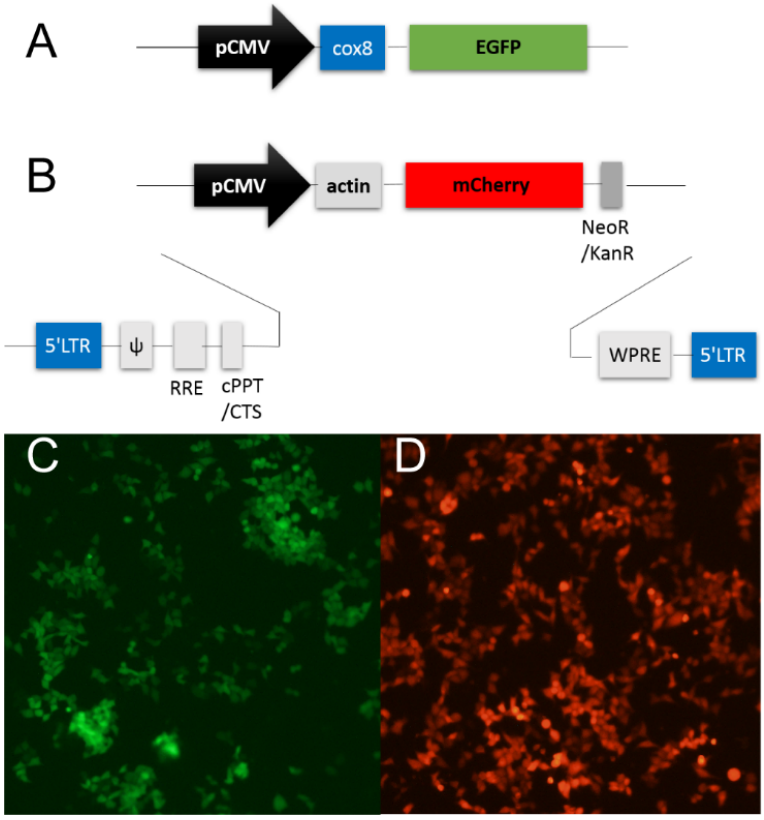

Figure 1.

A. Schematic illustration of the pEGFP-cox8 reporter system.

B. Schematic illustration of the pLVX-actin-mCherry reporter system.

C. Fluorescence images of HeLa cells transfected with EGFP-tagged COX8.

D. Fluorescence images of HeLa cells transfected with mCherry-tagged Actin.

To establish the cell line stably co-expressing COX8-EGFP and ACTIN-mCherry, we transfected the HeLa cells with the plasmid containing the expression sequence of COX8-EGFP, and obtained the COX8-EGFP expression cells. After screening by G418 for 2 weeks, the stably transfected cell line was obtained. The COX8-EGFP-mCherry-ACTIN co-expressing HeLa cell line was further established based on the COX8-EGFP expressing cells with lentiviral transfection system. Fig 1 shows the fluorescence microscope examination of the cells, confirming the co-expressions of COX8-EGFP and mCherry-ACTIN.

In order to further confirm the GFP expression right on the targeted mitochondria, we then labeled the mitochondria with TMRE dye in the GFP-tagged cells and then examined the dye-stained cells with a confocal microscope. As shown in Figure 2, the

165 COX8 protein fluorescence (Green) proteins and mitochondrial fluorescence (Red)
166 were indeed co-localized in the cells.

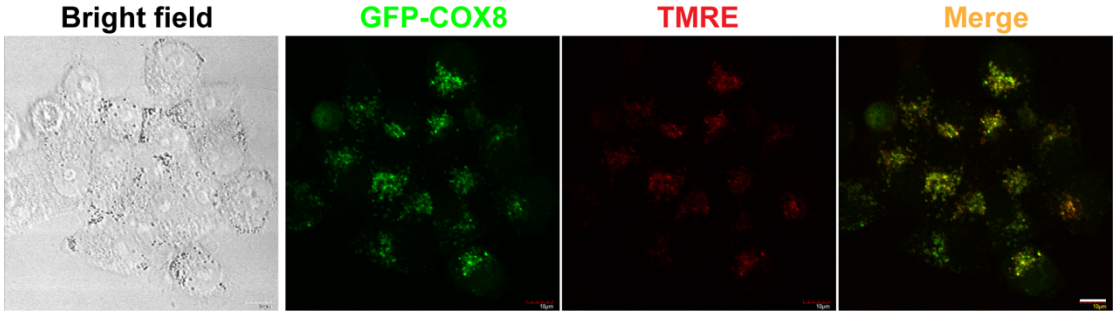

167

168 **Figure 2.**

169 Confocal microscopy observation of co-localization of GFP-COX8 on the mitochondria. The
170 GFP-COX8-HeLa cells were stained with TMRE (200 nM) for 20 minutes and before the
171 examination by confocal microscopy. Scale bar: 10 μm.

172 Furthermore, in order to verify the universal validity of our as-constructed dual
173 fluorescence reporting system for observing mitochondrial biogenesis, we also used
174 mitochondrial biogenesis's initiator 5-Aminoimidazole-4-carboxamide ribotide
175 (AICAR) as for the in-depth testing, or, as the positive control(Komen & Thorburn,
176 2014). The applied drug concentration was 0.5 mM. As shown in the Fig 3A-D,
177 compared with the non-AICAR treatment group, the AICAR treated group showed
178 increased fluorescence ratio with time. This experiment therefore confirmed that the
179 dual fluorescence system we constructed is feasible and effective for monitoring
180 mitochondrial biogenesis.

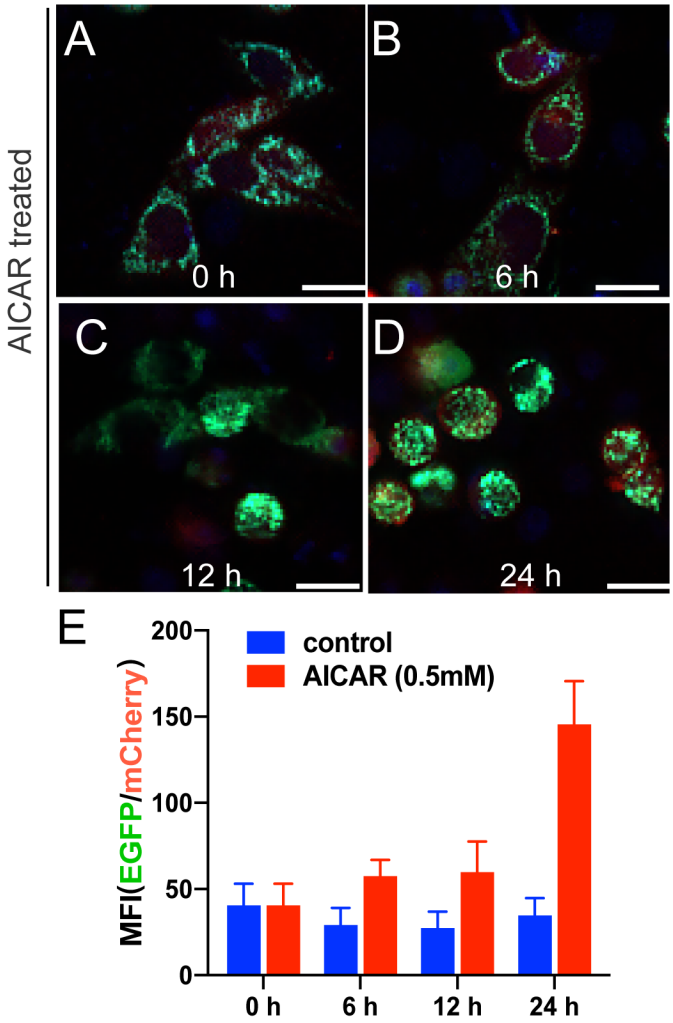

Figure 3.

A-D. The cells were treated with mitochondrial biogenesis inducer drug (AICAR, 0.5 mM) and observed with high-content imaging and screening (HCS) system after different treatment hours. In the figures, green color indicates the mitochondria encoding COX8-EGFP, red color shows the actin encoded by actin-mCherry, and blue color represents the DAPI stained nuclei. Scale bar: 25 μm.

E. The mean fluorescence intensity (MFI) ratios of HeLa cells treated by AICAR after different hours, in comparison with the non-AICAR treated cells as the control group. Bar graphs are presented as mean ± sd, n = 3.

Moreover, in order to further validate the effectiveness of the as-constructed fluorescent reporter system, we also testified the co-expression levels of GFP protein

together with the mitochondrial target protein (e.g. COX8) for the positive control with the cells treated by AICAR. Technically, CytoC was measured in the experiment instead of COX8 as COX8 is the subunit of CytoC. As shown in Fig 4, both GFP and CytoC were in the same trend of expression of levels for the mitochondrial biogenesis proteins including PGC1-α, NRF1 and TFAM. Besides, we also examined the AICAR-induced bio-marker proteins expression levels related to mitochondrial biogenesis. Fig. 4 shows that for the cells treated with AICAR, the expression levels of GFP, CytoC, PGC1-α, NRF1 and TFAM increased significantly in comparison with the untreated group. Also, with the increase of AICAR treatment time, the protein expression levels of mitochondrial biogenesis marker proteins (PGC1, NRF1, TFAM) also increased concomitantly (see Fig EV1). All these results therefore confirmed the validity of our fluorescence report system suitable for mitochondrial biogenesis monitoring.

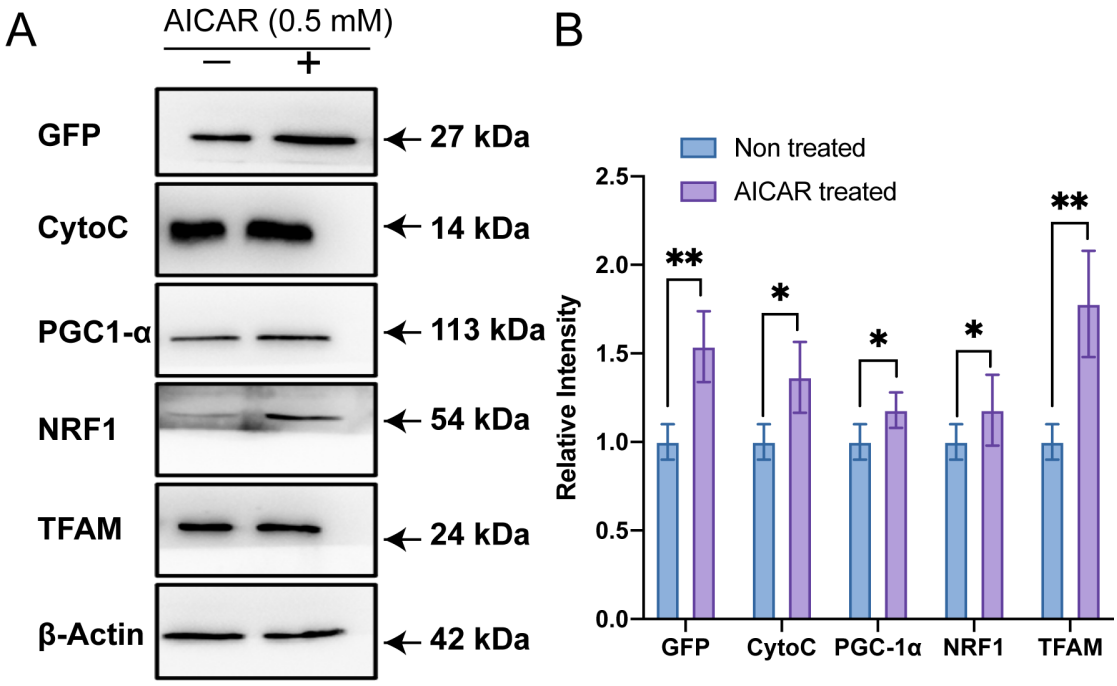

Figure 4.

A. HeLa cells were treated with mitochondrial biogenesis inducer drug (AICAR, 0.5 mM).

209 Total proteins were extracted after 12 hours.

210 B. The graph shows the comparison of the relative intensity for expressions of GFP and
211 mitochondrial biogenesis marker proteins between the non-AICAR treated group and the
212 AICAR treated group.

213 In-situ observation of the dual fluorescence reporter system for the evaluation of 214 the radiation-induced mitochondrial changes

215 With the establishment of this dual-fluorescence reporter system, we then employ
216 the laser fluorescence confocal microscope to observe the biological effect in the living
217 cells with the treatment of gamma-ray irradiation. The COX8-EGFP encoding
218 mitochondria (Green), the ACTIN-mCherry encoding actin (Red), and the DAPI-
219 stained nuclei were observed. The representative images together with the
220 corresponding quantitative analysis of fluorescence intensity are shown in Fig 5.

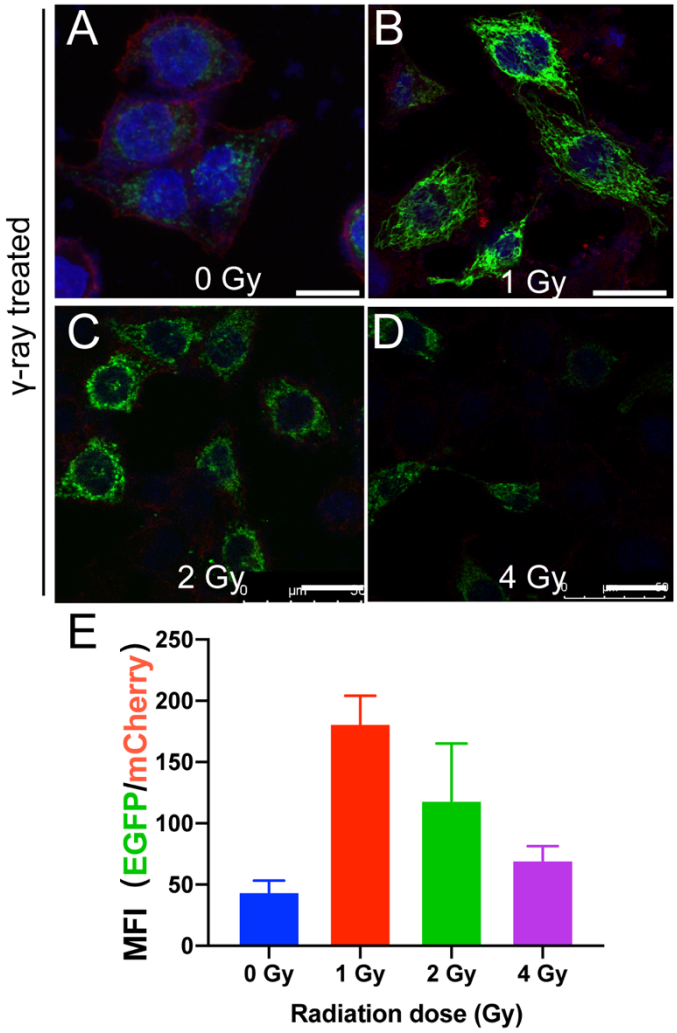

Figure 5.

A-D. HeLa-cox8-EGFP-actin-mCherry cells were exposed to 1 Gy, 2 Gy, 4 Gy gamma-ray and incubated for 24 h and observed with confocal laser scanning microscope. Green color indicates the mitochondria encoding COX8-EGFP, red color shows the actin encoded by actin-mCherry, and blue color represents the DAPI stained nuclei. Scale bar: 25 μm.

E. The ratio comparison for the mean fluorescence intensity (MFI) of GFP over mCherry fluorescence intensities quantified in the figure 2A-D. The MFI was determined by ImageJ software. Bar graphs are presented as mean ± sd, n = 3.

Fig 5 presents the fluorescent images of the cells by confocal microscopy, indicating that the intracellular mitochondrial content increased with radiation dose. Compared with the control group (0 Gy), the irradiated group showed mitochondrial

234 fluorescence enhancement, and it was significantly enhanced especially for the 1 and 2
235 Gy cases (Fig 5A-D). The fluorescent images intuitively show that the number of
236 mitochondria increased with increasing radiation dose, confirming that the dual
237 fluorescence reporter system can directly reflect the relevant mitochondrial responses
238 and changes in the living cells.

239 To investigate the mitochondrial fluorescence enhancement of the cells exposed to
240 ionizing radiation, the mean fluorescence intensity (MFI) from the dual fluorescence
241 reporter system was utilized. This MFI ratio change was also obtained by employing
242 the High Content Imaging and Screening (HCS) system, with the results shown in Fig
243 6. The HCS living cell workstation recorded the changes of cell fluorescence within 24
244 hours after cell irradiation (the videos were also recorded, see Videos S1, S2, S3 in the
245 Supporting Information). The results indicate that for 1 Gy, the fluorescence ratio
246 GFP/mCherry increased with time, while for 2 Gy and 4 Gy cases, the fluorescence
247 ratio increased significantly with the irradiation dose during the first interval of 1-12
248 hours, but afterwards, it decreased to some extent, though still higher than that of the
249 control (non-irradiated cells). The reduction in MFI suggested that the mitochondria of
250 the irradiated cells with higher radiation doses were actually more detrimentally
251 damaged by the radiation than that received lower radiation doses. Fig EV2 shows the
252 numerical changes of two fluorescence channels detected by flow cytometry. The MFI
253 ratio of $EGFP^{+}$: $mCherry^{+}$ was calculated, and it was found that the fluorescence ratio
254 was positively correlated with the radiation dose. So the result by the flow cytometry

255 (Fig EV2) also confirms there were significant differences between the irradiated and

256 non-irradiated groups.

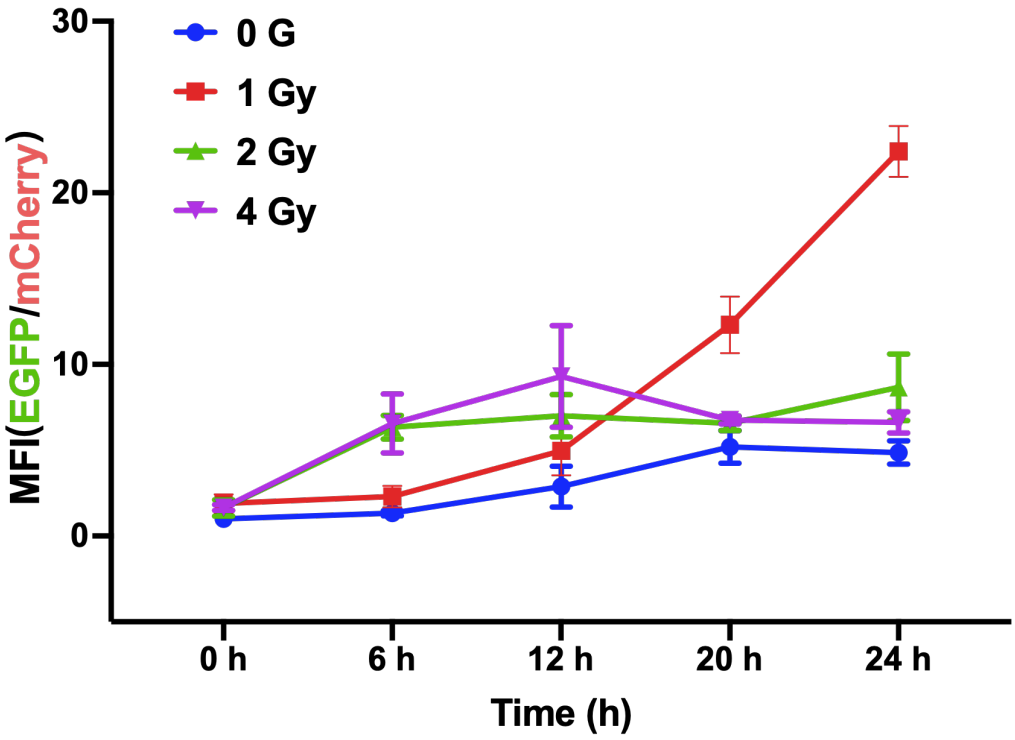

257

258 **Figure 6.**

259 The cellular mean fluorescence intensity (MFI) measured by High Content Imaging and

260 Screening (HCS) system. HeLa-Cox8-EGFP-actin-mCherry cells were exposed to 1 Gy, 2 Gy,

261 and 4 Gy gamma-ray respectively. MFI changed with time after the γ-ray irradiation.

262 **Radiation effect on cell viability, survival rate, cell cycle, apoptosis, DNA damage**

263 **and mitochondrial membrane damage**

264 To investigate the radiation effect, the cell viability was measured by CCK-8

265 method, showing that the cell viability decreased with the increase of radiation dose

266 (Fig 7A). The toxic effect of radiation on cells was also examined using LDH kit, which

267 revealed that the radiation-induced toxicity was indeed increased significantly with

268 radiation dose (Fig 7B). Also, the colony-forming method was used to analyze the

inhibitory effect of γ-ray on HeLa cell survival. With increase of γ-ray irradiation dose, the cell survival rate was only 30% after 4 Gy irradiation (Fig 7C), confirming that the cell survival rate decreased with the rise of radiation dose.

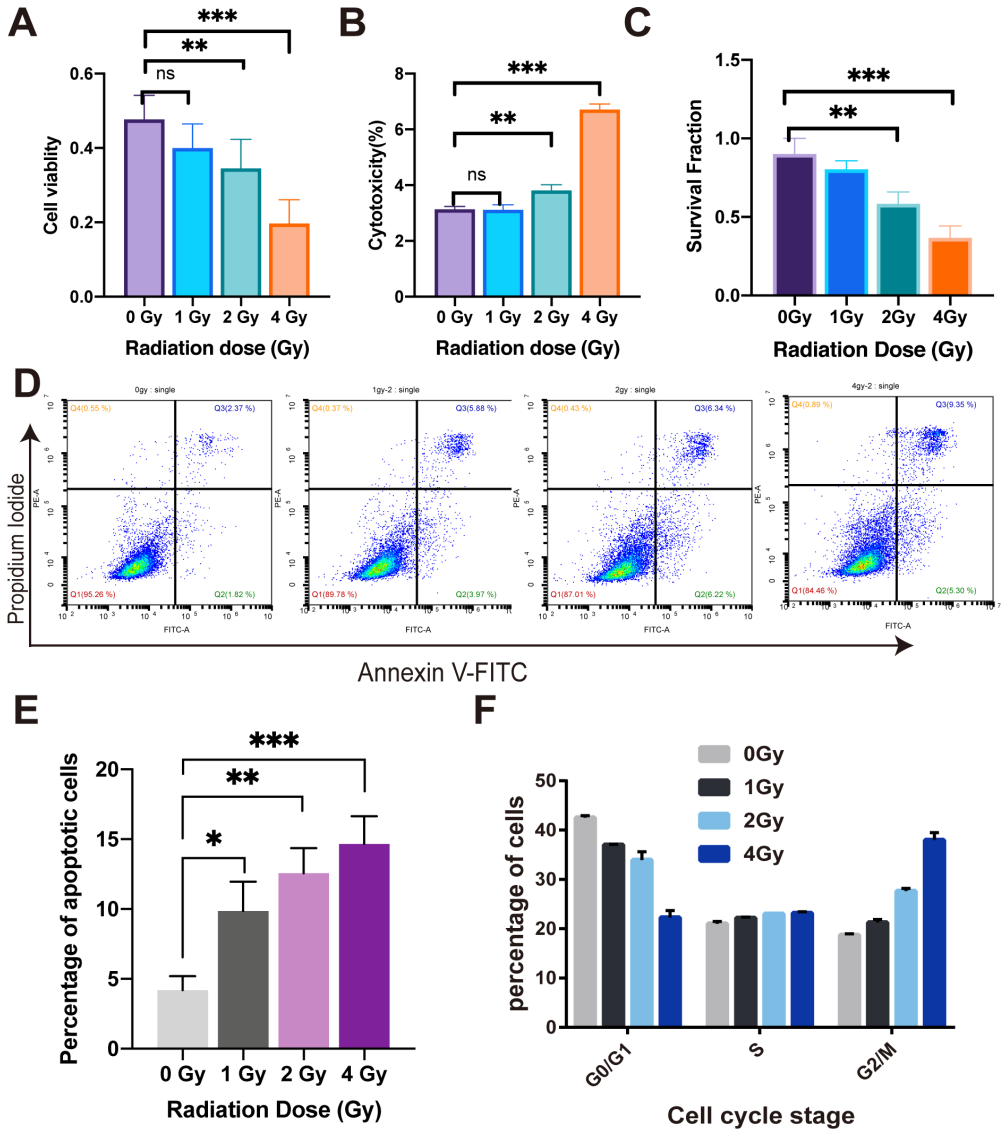

Figure 7.

A. CCK-8 assay for cell viability.

B. LDH assay for cell cytotoxicity.

C. Colony formation assay of HeLa cells after 14 days under different radiation doses.

D. Flow cytometry results of Annexin V-PI assay.

E. Apoptotic cells at different radiation doses.

F. Cell cycle examination. The experiment was performed 3 times. Data are presented as

Mean±SD; $P < 0.01$(**); $P < 0.001$(***); ns: not significant compared with untreated cells.

In addition, the cell cycle and apoptosis were assessed for the cells irradiated with γ-ray. Apoptotic cells were detected by flow cytometry after irradiation using Annexin V-PI methods (Fig 7D). Through statistics and comparison of the number of apoptotic cells, it was found that with the increase of radiation dose, the number of apoptotic cells increased significantly (Fig 7E). Cell cycle was analyzed by flow cytometry, and the results showed that all groups of cells had G2 arrest after 24 hours of irradiation, especially at 2 Gy and 4 Gy irradiation doses showed significant G2 arrest (Fig 7F).

Furthermore, in order to understand the radiation effects, the radiation induced damages on DNA and mitochondrial membrane, together with the accompanied ROS levels were also examined. For such a purpose, the immunofluorescence method was used to detect DNA damage, H_2DCFDA probe was used to label ROS, and TMRE was used to label mitochondrial membrane potential. Fig 8A shows that with increase of the radiation dose, the foci of the γ-H2AX increased significantly, and the statistical results showed that the ROS level in the irradiated cells increased with the increase of the radiation dose (Fig 8B- D). At the dose of 2 Gy, the ROS level was the highest, and for the 4 Gy group, there was a significant difference compared with the non-irradiated group. In the meantime, the mitochondrial membrane potential decreased significantly with the increase of radiation dose (Fig 8E, F).

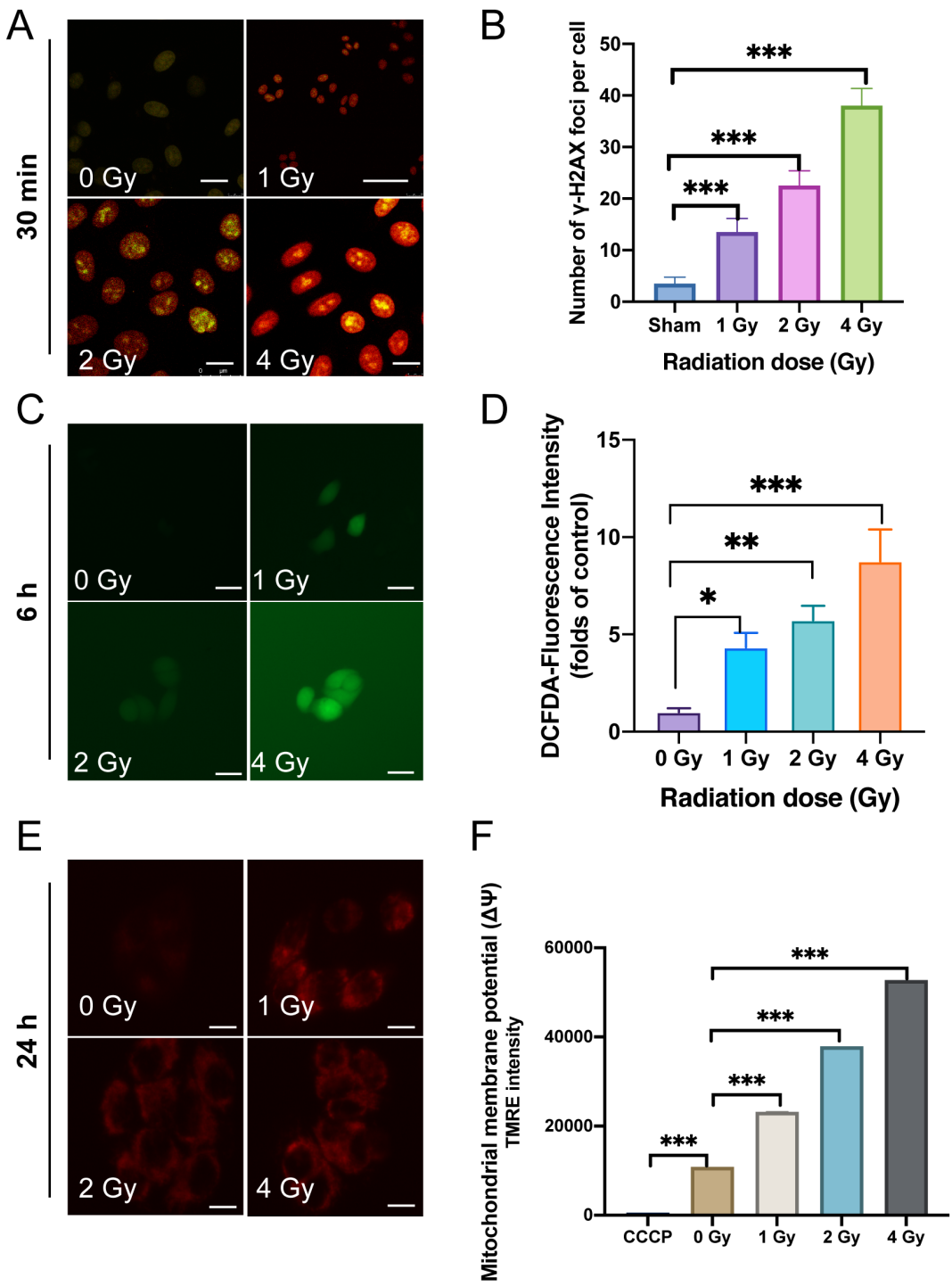

Figure 8.

A. Representative images for DNA damage measured instantly (within 30 minutes) after the Hela cells were exposed to radiation with different radiation doses. Green: γ-H2AX; red: DNA stained with PI; Scale bars: 20 μm.

B. The graph shows the percentage of population with the noted number of γ-H2AX foci with different irradiation doses.

306 C-D. ROS assessment using H_2DCFDA assay at 6 h.

307 E- F. MMP assay using TMRE at 24 h.

308 As the ionizing radiation induced DSB of DNA, we expected that there would also
309 be enhanced DNA repair process in the irradiated cells. Indeed, we observed the
310 fluorescence from γ-H2AX and the co-localization of 53BP1 foci after the radiation
311 exposure. Fig 9 shows the number of foci increased significantly with the increase of
312 radiation dose, while the number of foci of 53BP1 was the largest at 1 Gy but then
313 decreased with radiation dose, implying that at higher radiation dose the cell received
314 severer damage son the DNA repair ability became weaker.

315

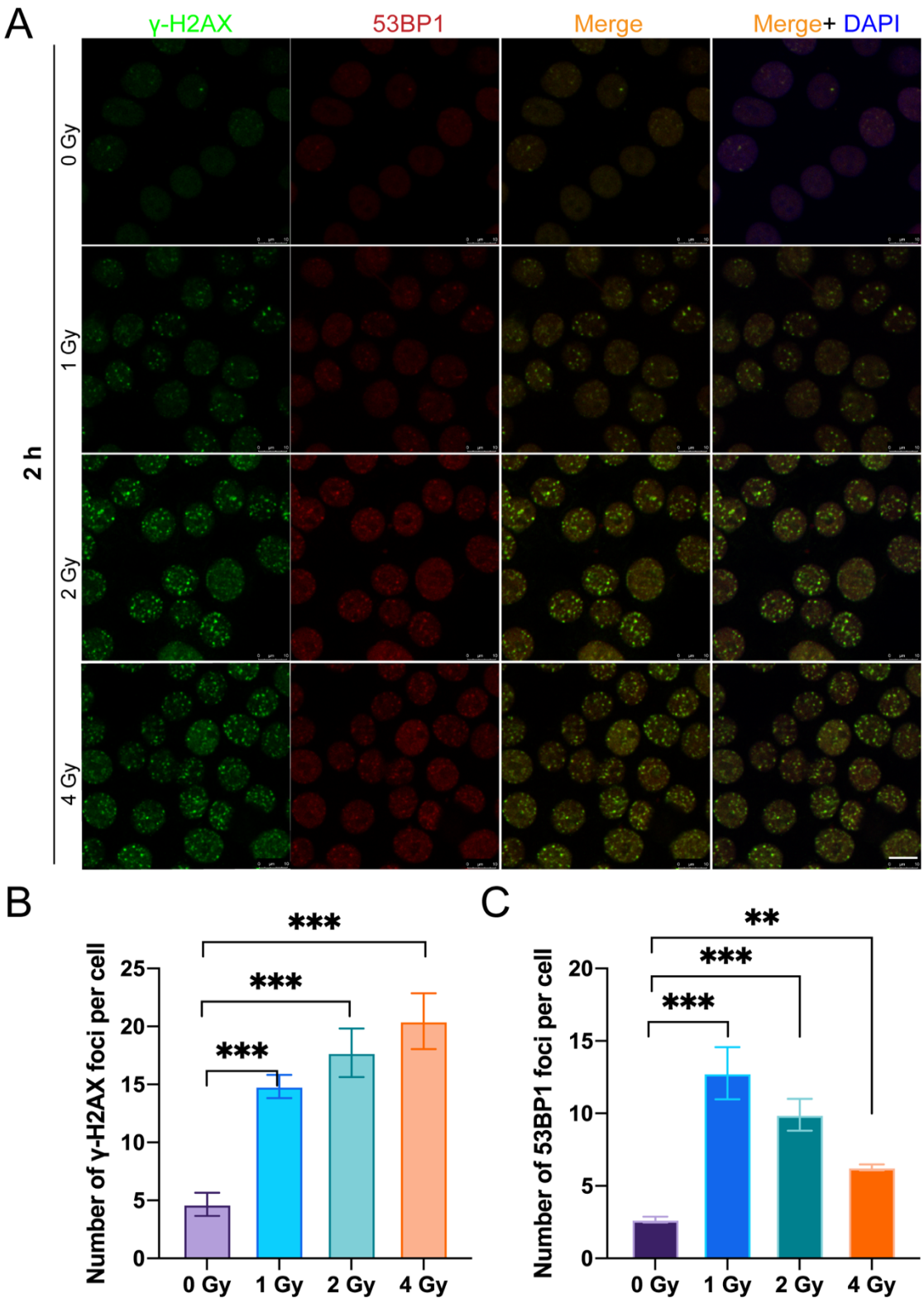

Figure 9.

A. Representative images for DNA damage detection when the cells were exposed to radiation with different radiation doses. Green: γ-H2AX; red: 53BP1; Blue: DNA nucleus stained with DAPI; Scale bars: 10 μm.

321 B. The percentage of population with the noted number of γ-H2AX foci corresponding to the
322 respective fluorescence images.
323 C. The percentage of population with the noted number of 53BP1 foci corresponding to the
324 respective fluorescence images. At least 100 nuclei per genotype were used for
325 quantification. Image auto-quantification was performed with CellProfiler version 4
326 (www.cellprofiler.org).
327

Verification of mitochondrial biogenesis and apoptosis

To further verify the mitochondrial biogenesis induced by radiation, the copy number of mitochondrial DNA was evaluated. Total DNA was extracted from HeLa cells 6-24 hours after irradiation. As shown in Fig 10, the copy number of mitochondrial DNA changed significantly after cell irradiation. Indeed, under the same radiation dose, mitochondrial DNA number increased significantly compared with that of the non-irradiated cells.

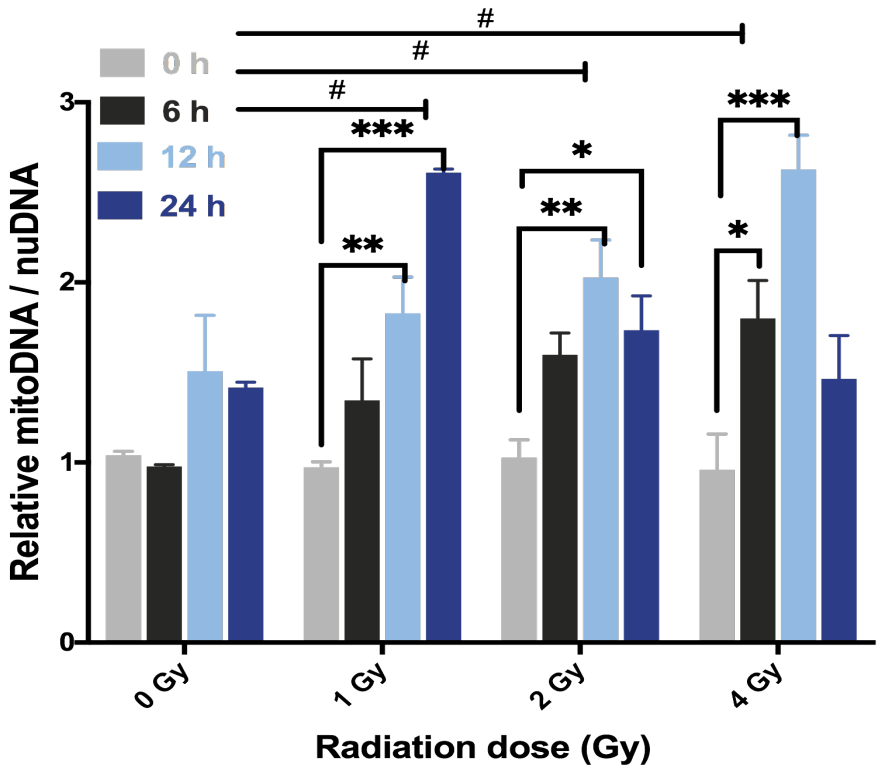

Figure 10.

Effect of gamma-irradiation on mitochondrial DNA copy number. HeLa cells were exposed to gamma rays at doses of 1 Gy, 2 Gy and 4 Gy. After 6, 12, 24 hours, total genomic DNA was extracted and used as a template to detect the mtDNA/nDNA ratio by RT-qPCR. Data are presented as Mean±SD; #: significant compared with unirradiated group; $^{**}P<0.01$; $^{***}P<0.001$.

342 Furthermore, to explore the correlation between mitochondrial biogenesis and
343 apoptosis under the condition of radiation, the related marker proteins were also
344 examined. For the mitochondrial change, the related protein expression levels of PGC-
345 1α, NRF1, TFAM and Mfn1 at different times (6 h, 12 h, 24 h) with different radiation
346 doses (0 Gy, 1 Gy, 2 Gy, 4 Gy) were assessed by Western blots (Figure 11). At 6 hours,
347 the expression level of TFAM protein was increased with radiation dose. On the other
348 hand, for the apoptosis, the related protein expression levels of apoptosis-related marker
349 proteins (BAX, Bcl-2, CytoC, Caspase-3, Cleaved Caspase-9, PARP) were examined.
350 As shown in Figure 8, the expression levels of crucial apoptosis proteins did not differ
351 significantly at early time (6 h), but their expression levels increased significantly
352 afterwards (12 h, 24 h). So these results unambiguously demonstrate that the
353 mitochondrial biogenesis at early time (6 h) was indeed positively correlated to the
354 apoptosis in the late stage (24 h).

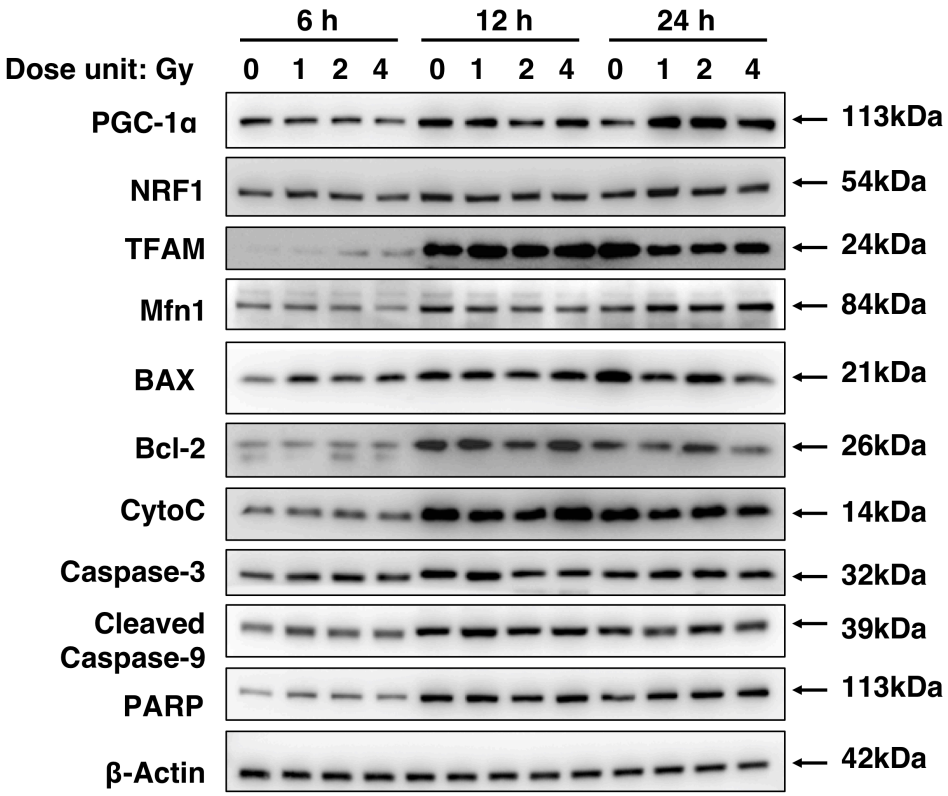

Figure 11.

Western blot (WB) assay of the related proteins after radiation treatment. HeLa cells were treated with different doses of irradiation (0, 1, 2, 4 Gy), and total proteins were extracted at different time points. The WB assay shows the changes of expression of mitochondrial biogenesis marker proteins (PGC-1α, NRF1, TFAM and Mfn1) and apoptotic marker proteins (BAX, Bcl-2, CytoC, Caspase-3, Cleaved Caspase-9, PARP) with time.

Discussion

Mitochondria as the cell energy factory play a vital role in cell homeostasis(Lill & Freibert, 2020). In response to external stimuli, mitochondrial biogenesis can be elicited in order to provide the cells with extra energy(Barros & McStay, 2019). Previously, many studies had reported that mitochondrial biogenesis could suppress apoptosis(Yu *et al*, 2013), i.e., there would be negative correlation between mitochondrial biogenesis and apoptosis. Generally, these studies mainly concerned the cell response to relatively small stimulus or stress. But what would happen if the external stimulus or stress is

370 large enough so that the final fate of cell death or apoptosis cannot be avoided? Would
371 mitochondrial biogenesis still go along with apoptosis in this case? And if there would
372 be mitochondrial biogenesis occurring as the early event of the apoptosis, how would
373 it change with time? With these questions, we thus initiated this research, and applied
374 radiation approach to induce both mitochondrial biogenesis and apoptosis in the cells,
375 so as to explore the time-dependent relationship between mitochondrial biogenesis and
376 apoptosis. As a result, we have achieved the following results with some new findings
377 and elaborated understandings.

378 Firstly, we have constructed the dual fluorescence report system that can be
379 effectively used for mitochondrial biogenesis study. To probe the changes taking place
380 in mitochondria, we especially developed the approach using mitochondrial-tagged
381 recombinant fluorescent proteins. The fluorescent protein reporting system has the
382 advantages of real-time, convenient, fast, and non- destructive(Betzig *et al*, 2006). Besides,
383 it has also an advantage in the study of subcellular organ localization and protein stress
384 regulation(Llopis *et al*, 1998). Previously, people often used fluorescent dye probes for
385 studying effect involved with mitochondria. For example, Mukhopadhyay et al. used
386 Annexin V and Sytox Green and MitoSOX Red fluorescent probes to study the
387 detection of apoptosis and mitochondrial superoxide so as to establish the method for
388 detecting living cells by laser confocal scanning microscopy and flow cytometry
389 (Mukhopadhyay *et al*, 2007). But the disadvantages of fluorescent dyes are the toxicity to
390 cells, as well as the light quenching under long-period real-time observation. Compared
391 to fluorescent dyes, fluorescent proteins are more stable and have minimal toxicity and
392 can generate visible fluorescence in vivo (Westermann & Neupert, 2000). Actually, GFP

393 reporter protein is now commonly used to detect mitochondrial changes(Mahajan *et al*,
394 1998; Hanson *et al*, 2004). In this work, in particular, we constructed the dual
395 fluorescence reporting system based on fluorescence proteins for monitoring the
396 mitochondrial biogenesis process. In order to verify the effectiveness of this system
397 designed for monitoring mitochondrial biogenesis, in this study, we applied AICAR to
398 activate mitochondrial biogenesis as the positive control (Komen & Thorburn, 2014).
399 AICAR is an activator of AMP-activated protein kinase (AMPK) that can permeate cell
400 membranes(Rai *et al*, 2015). Among them, AMPK (AMP activated protein kinase) is
401 an activator of mitochondrial biogenesis and key regulator of energy homeostasis
402 caused by external factors(Kim *et al*, 2016). The main function is to phosphorylate
403 PGC-1α protein, or affect the transduction of SIRT1 signaling pathway(Mihaylova &
404 Shaw, 2011). Our result clearly showed that AICAR indeed induced the up-regulation
405 of key protein levels of mitochondrial biogenesis, confirming that the as-constructed
406 dual fluorescent protein reporter system could track the event of mitochondrial
407 biogenesis effectively. Also, this dual fluorescent protein reporter system is not only
408 suitable for the real-time in situ observation for a long time, but also facilitates the
409 precise fluorescence evaluation with the reference fluorescent protein for intensity
410 normalization. Therefore, by analyzing the ratio of the fluorescence intensity of
411 mitochondrial DNA to that of nuclear DNA expression, the early event of mitochondrial
412 biogenesis under irradiation condition could be readily observed and evaluated, and
413 with this approach we could thus sensitively track the early process that which
414 eventually led to the late event of apoptosis.

415 Secondly, with the as-constructed dual fluorescence report system, we have
416 observed the radiation-induced mitochondrial biogenesis together with the apoptosis.
417 Ionizing radiation has been used for cancer therapy for they can directly or indirectly
418 cause DNA damage and kill the cancer cells(Spitz *et al*, 2004). With DNA damage in
419 the nucleus, cells may undergo cell cycle arrest required for repairing the damage or
420 cell death including apoptosis(Bernstein *et al*, 2002). In parallel, mitochondria is also
421 considered to be involved in the radiation induced effects, where more reactive oxygen
422 species (ROS) would be produced which may affect the cells profoundly. Actually, it
423 has been well documented that exposure of cells to ionizing radiation could activate
424 ROS to produce oxidases, regulate antioxidants, and alter metabolic activity in response
425 to oxidative damage(Azzam *et al*, 2012). In both the nucleic or mitochondrial processes,
426 more ATP is required to elicit mitochondria biogenesis either directly or indirectly(Kulms
427 *et al*, 2002; Srinivas *et al*, 2019). So it is not surprising that mitochondria biogenesis could
428 take place as one of the consequences of radiation-induced bio-effects (Galluzzi & Kroemer,
429 2008). But interestingly, in our fluorescence measurements, we found that the
430 fluorescence ratio increased and reached the maximum at 6 h after irradiation, but
431 afterwards the fluorescence ratio decreased gradually. According to our established
432 mitochondrial fluorescence report system, this suggests that in the early stage,
433 mitochondrial biogenesis was indeed initiated and enhanced. In this process of
434 mitochondrial biogenesis, mitochondrial DNA and mitochondrial mass were
435 maintained to keep the cell homeostasis and metabolism(Huangyang *et al*, 2020). But in
436 the late stage of the radiation effect, the fluorescence ratio decreased, showing that the

437 function of mitochondrial biogenesis gradually diminished. We can also understand this
438 change by relating it to the ROS elevation. There was increase of ROS caused by
439 radiation, which continuously increased the oxidative stress and damaged the mtDNA
440 and the mitochondrial integrity. For the role of ROS, it is generally accepted that normal
441 range of ROS may induce stress response by changing the expression of related nuclear
442 genes, and certain level of ROS can save cells by maintaining energy metabolism
443 (Srinivas et al., 2019); but when the ROS level exceeds the tolerant threshold, ROS can
444 then induce the transition of mitochondrial membrane permeability, leading to the
445 activation of the caspase pathway and promoting cell apoptosis. In our experiment, we
446 indeed detected the increase of ROS level and the decrease of mitochondrial membrane
447 potential. Also, given the increase of radiation dose, we detected the related caspase
448 related proteins and found that the increase of pro-apoptotic proteins such as
449 cytochrome c. Release of cytochrome c is an indicator for the apoptosis, in which the
450 oxidative stress would damage mtDNA and other components of the cells(Lee & Wei,
451 2005). Here, we especially notified that the mitochondrial fluorescence intensity change
452 rates were quite different after the cell exposure to the radiation. The larger the
453 irradiation dose, the higher the fluorescence ratio reduction rate. All these observations
454 are actually the typical features for the radiation-induced apoptotic process.

455 Thirdly, our new observation have revealed the more subtle but very important
456 relationship which had largely been ignored by previous studies. We noticed that in the
457 beginning of the process, the mitochondrial biogenesis was actually increasingly
458 associated with the apoptotic stress, and the trend of fluorescence change was consistent

459 with the number of apoptotic cells. This is actually contrary to the conventional view
460 on the relationship between mitochondrial biogenesis and apoptosis. In the past, there
461 were few reports concerning the dynamic process of mitochondrial biogenesis, and the
462 mainstream opinion or understanding on the relationship between mitochondrial
463 biogenesis and apoptosis was that these two processes normally appear to be
464 antagonistic. For example, many studies showed that the apoptosis occurred
465 simultaneously with the suppression, or, that apoptosis took place with even missing
466 the observation of mitochondrial biogenesis (Martins *et al*, 2015; Vayssiere *et al*, 1994;
467 Zhang *et al*, 2017; Lin *et al*, 2020). This is actually not true or accurate, because
468 mitochondrial biogenesis as an earlier event did occur preceding the late state of
469 apoptosis, as we clearly demonstrated in this study.

470 The reason for this misleading of understanding is largely due to the ignorance of
471 the investigation of the dynamic process of the cells. In the past, people tended to
472 choose just several time check points for inspecting the apoptosis and mitochondrial
473 biogenesis. But which time check points are most suitable for the correct evaluation?
474 What cautions should be taken to avoid the wrong evaluation when especially
475 concerning the relationship between the processes in the involvement? To solve this,
476 we actually need to establish more advanced method to studying the cellular effect in
477 its dynamic process, and so to scrutinize the processes of both mitochondrial biogenesis
478 and apoptosis in their logical time sequence. This is simply just one of the main
479 purposes of this study. It is understandable why people had not focused on the study of
480 processes, as we realized that there had been lack of tool/method for the monitoring the

481 whole process regarding the mitochondrial changes in situ and in a nondestructive way.
482 For example, the traditional methods include using real-time quantitative PCR to detect
483 the copy number of mitochondrial DNA, or using Western blot assay to identify the
484 changes of marker protein level of mitochondrial biogenesis. These methods cannot
485 achieve in-situ and real-time observation in living cells. On the contrary, the
486 fluorescence protein method can be used to observe the mitochondrial biogenesis in
487 real time as especially useful for studying the early events prior to apoptosis. Therefore,
488 in this work, we at first attempted to construct the fluorescent reporting system which
489 could let us to track the change of mitochondrial biogenesis. Based on the fluorescence
490 signal, the dual fluorescence ratio can help us to predict the radiation effects or the cell
491 fate according to the fluorescence change of these irradiated cells. In particular, from
492 the fluorescence data obtained from Fig 6, we can calculate the fluorescence ratios, and
493 so we can retrieve the MFI ratios in each irradiation dose group (0 Gy, 1 Gy, 2 Gy, 4
494 Gy) at an early time, as shown in Fig 12 A&B. Strikingly, this result is consistent with
495 the cells in the apoptotic state at 24 h (Fig 7E). In the late stage (24 hours), the
496 fluorescence ratio becomes smaller as the irradiation dose increases. It is
497 understandable because the apoptosis is actually dependent on the early biochemical
498 events in the cells(Holler *et al*, 2000). In this way, we may therefore infer or predict the
499 late apoptotic state of cells by observing the early-staged changes in terms of
500 mitochondrial fluorescence ratio. On the other hand, it is also seen that this fluorescence
501 ratio was significantly reduced after 24 h (Fig 12C), which is not concomitant with the
502 apoptosis at 24 h (Fig 7E). This suggest that it is very critical to evaluate both the

503 processes by choosing the right time check points.

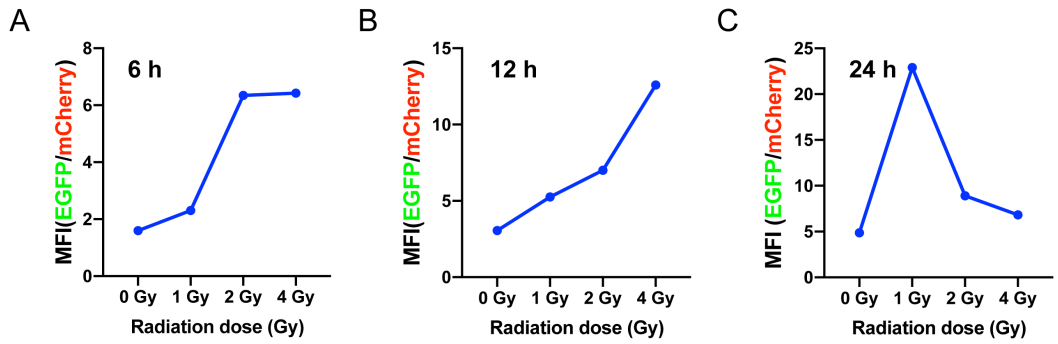

504

505 **Figure 12.**

506 Analysis of mitochondrial biogenesis and apoptosis.

507 A. Analysis of EGFP/mCherry ratio in High Content Screening (HCS) at 6h.

508 B. Analysis of EGFP/mCherry ratio in High Content Screening (HCS) at 12 h.

509 C. Analysis of EGFP/mCherry ratio in High Content Screening (HCS) at 24 h.

510 Lastly, we have also tried to understand the mechanism for the mitochondrial
511 biogenesis related to the radiation-induced apoptosis. Generally, it is believed that the
512 biogenesis of mitochondria is a very complex biological process, which can maintain
513 the cell homeostasis by controlling the self-renewal of subcellular organelles and
514 maintaining mitochondrial DNA (Scarpulla, 2008). The initiation of mitochondrial
515 biogenesis is normally triggered by the reception of energy demand signals caused by
516 external stress (Popov, 2020), while at the same time, mitochondrial biogenesis itself is
517 a protection way for cell's self-renewal. Since it is well-known that ionizing radiation
518 is an effective way to stimulate the cell mitochondrial biogenesis, we thus employed
519 the tool of ionizing radiation to treat the cells. As a result, we have successfully proved
520 that some marker proteins of mitochondrial biogenesis are involved in the biological
521 effects of radiation. We have found that the protein expression levels of nuclear
522 respiratory factor1 (NRF1), peroxisome proliferative activated receptor, gamma,

523 coactivator 1 alpha (PGC-1α), transcription factor A, mitochondrial (TFAM) increased
524 with radiation dose. NRF1 is a transcription factor with a vital role in mitochondrial
525 functional genes(Virbasius *et al*, 1993). PGC-1α is a transcriptional coactivator which is a
526 key inducer of mitochondrial biogenesis (Wu *et al*, 1999). TFAM is a key activator
527 of mitochondrial (mt) DNA transcription. mtDNA is reported to be very susceptible to
528 oxidative stress(May-Panloup *et al*, 2005). With the confirmation of these factors, we have
529 thus also again unambiguously confirmed that this mitochondrial biogenesis is indeed
530 related to radiation-induced cell adaptation and apoptosis.

531 But how to explain the suppression or disappearance of mitochondrial biogenesis
532 for the higher dose of radiation observed in the late stage of the cell process which
533 corresponds to the apoptosis? In our experiments, we observed that mitochondrial
534 biogenesis increased in the early stage of the cell process, but with the increase of
535 radiation dose, the mitochondrial biogenesis decreased substantially in the late stage.
536 We speculate that this change of mitochondrial biogenesis is related to DNA repair
537 ability. It was previously reported that mitochondrial biogenesis can enhance DNA
538 repair ability, and mitochondrial biogenesis is closely related to DNA repair ability(Li
539 *et al*, 2020) (Fu *et al*, 2008). For example, it was reported that doxorubicin, a drug
540 which can induce DSBs of DNA as accompanied by mitochondrial biogenesis (Kluza
541 *et al*, 2004). Normally, there are two main repair pathways of DSBs in mammalian cells:
542 non homologous end joining (NHEJ) and homologous recombination mediated repair
543 (HR) (Löbrich & Jeggo, 2005). Mitochondrial biogenesis can promote DNA repair by
544 inducing chromatin changes in DSB and regulating the activity of DNA repair factors,

545 and this upstream factor has be found to be the silent information regulator (SIRT)
546 (Paredes & Chua, 2016). SIRT is a family of sirtuins that depend on NAD^+ lysine
547 deacetylases, which may play an important role in mitochondrial biogenesis and cell
548 metabolism(Chalkiadaki & Guarente, 2015). On the other hand, DSB repair can be
549 achieved by NHEJ which can activate DNA-PK (Davis *et al*, 2014), while DNA-PK
550 can activate AMPK signal pathway, which is just closely related to mitochondrial
551 biogenesis (Park *et al*, 2017). In our experiment, we have indeed observed the change
552 of DNA repair as reflected by the change of 53BP1, and this change is just concomitant
553 with the mitochondrial biogenesis.

554 So, with the above findings and discussion of mechanisms, we can therefore
555 concisely describe the process of radiation affecting cells as schematically depicted in
556 Fig. 13. After a certain dose of radiation, DNA damage occurs, and the cell cycle is
557 blocked in order to initiate the repair process. At the same time, radiation produces a
558 large amount of ROS in the cell and affects the homeostasis of the cell. To resist the
559 radiation stress or damage, mitochondria then start to provide more energy for DNA
560 repair and maintenance of cell metabolism and homeostasis, leading to mitochondrial
561 biogenesis. Next, as ROS continues to increase, mitochondrial damage occurs, leading
562 to the decrease in membrane potential, which finally leads to the release of the pro-
563 apoptotic protein cytochrome c, activation of the apoptosis caspase pathway, and so the
564 programmed cell death.
565

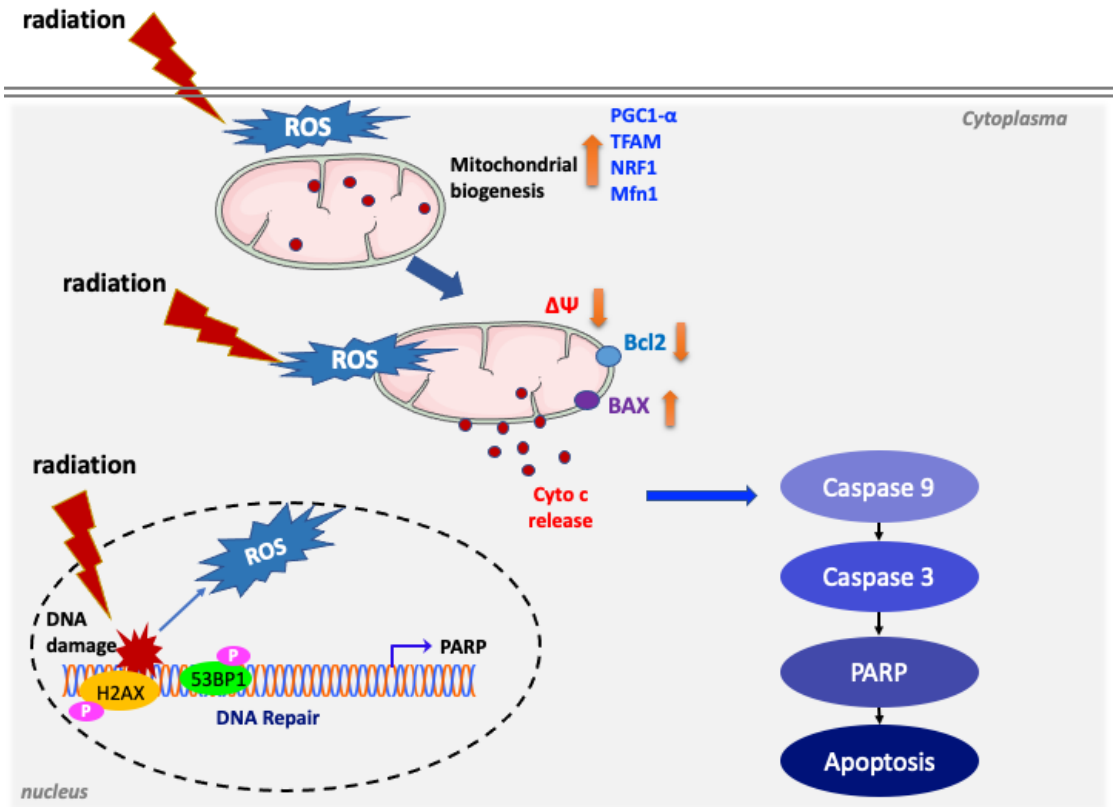

Figure 13.

Schematic diagram of biochemical events after ionizing radiation.

Conclusions

In this work, we have constructed a dual fluorescence reporter system for achieving the real-time observation of mitochondrial changes, which are related to mitochondrial biogenesis and apoptosis induced by ionizing radiation. Particularly, we have scrutinized the relationship between this mitochondrial biogenesis and apoptosis by considering the time sequence of occurrence, showing that these two processes are not antagonistic if they are evaluated at right time points. In other words, they may be positively correlated if we relate the mitochondrial biogenesis taking place at the early time to the apoptosis occurring at the late stage. Therefore, this work not only provides an effective method for directly observing the mitochondrial biogenesis process in

580 living cells, but also demonstrates how to evaluate the biological effects correctly with
581 right timing, with which we may thus be able to predict the cell fate such as apoptosis
582 through the cell's early event observation.

583 Materials and methods

584 Reagents

585 The *Escherichia coli* DH5a and DNA Ladder were purchased from Transgen
586 (Beijing, China). *Nhe*I, *Hind*III, *EcoR*I, *Not*I restriction enzymes, T4 DNA Ligase, and
587 Q5 High-Fidelity DNA Polymerase were purchased from NEB (MA, USA). Plasmid
588 pEGFP-N1 was purchased from Clonetech Biotechnology (CA, USA). Plasmid pLVX-
589 mCherry, PUC57 were stored in our laboratory. Plasmids of psPAX2 (# 12260) and
590 pMD.2G (#12259) were purchased from Addgene. PCR purification and gel extraction
591 kits were obtained from Axygen (CA, USA). TRIzol™ reagent, Lipofectamine 2000
592 were purchased from Invitrogen (CA, USA). Primescript II 1st strand cDNA Synthesis
593 Kit, RT-qPCR kit and Total genomic DNA extraction kit were purchased from
594 TAKARA (Dalian, China). G418, DAPI was purchased from Beyotime Institute of
595 Biotechnology (Shanghai, China). Reactive oxygen species (ROS) probe 2',7'-
596 dichlorodihydrofluorescein diacetate (H2DCFDA, D6883) was purchased from Sigma-
597 Aldrich. Tetramethylrhodamine ethyl ester (TMRE, T4057) was purchased from
598 Useverbright. 5-Aminoimidazole-4-carboxamide ribotide (AICAR) was purchase from
599 Selleck (MA, USA). The antibodies of PGC-1α, NRF1, TFAM, Mfn1, BAX, Bcl-2,
600 CytoC, Caspase-3, Cleaved Caspase-9, PARP, γH2AX(S139), GFP were purchased

601 from Bimake (MA, USA), 53BP1, anti-β-Actin antibody was purchased from CST (MA,
602 USA). Alexa Fluor® 488 Goat Anti-Mouse (IgG) secondary antibody, Alexa Fluor®
603 647 Goat Anti-Rat (IgG) secondary antibody were purchased from Invitrogen (CA,
604 USA).

605 **Creation of stably transfected cell lines**

606 **Generation of plasmids.** Firstly, the pEGFP-N1-COX8 expression plasmid was
607 constructed. Briefly, the DNA sequence of cytochrome c oxidase 8A subunit was found
608 from Genbank (NM_004074.2) (Hendrickson et al., 2010). Then two complementary
609 oligonucleotide strands were obtained by amplification using PCR, and the restriction
610 sites of the *Nhe*I and *Hind*III were added at both ends. The sequences of oligonucleotide
611 strands were listed in S1 Table. The DNA sequence (COX8A) was ligated on the PUC57
612 plasmid. Then, the appropriate oligonucleotides were annealed and ligated into pEGFP-
613 N1 cloning cut with *Nhe*I and *Hind*III. After incubation overnight at 37°C, the target
614 plasmids were extracted from the bacterial fluid using the EndoFree Maxi Plasmid kit.

615 Secondly, the PLVX-mCherry-Actin expression plasmid was constructed. Total
616 RNA was extracted from HeLa cells by Trizol reagent and served as the template for
617 cDNA synthesis, and then it was reversely transcripted using Primescript II 1st strand
618 cDNA synthesis kit. The primers were designed according to the sequence of actin
619 (Genbank no. NM_10277): *EcoR*I tailed forward (5′-
620 gtcGAATTCatggatgatgatatcgccgcgc-3′) and *Not*I tailed reverse (5′-
621 TATGCGGCCGCctagaagcatttgcggtggac-3′) primers which are named as Fw-actin-

622 EcoRI and Rv-actin-NotI, respectively. The length of the amplified product was 1128
623 bp. The PCR product was separated by electrophoresis, and the target fragment was
624 recovered after gel cutting and purification. The target gene fragment (actin) and the
625 expression vector (LVX-mCherry) with the same restriction site (*EcoR*I and *Not*I) were
626 digested by restriction enzymes respectively, and then ligated with T4 ligase and
627 transformed into *E. coli* DH5a for plasmid amplification.

628 **Production of lentiviral supernatant and transduction of COX8-EGFP-mCherry-**
629 **ACTIN-HeLa.** Briefly, positive monoclonal cells (COX8-EGFP-HeLa cells) were
630 constructed. When HeLa cells grew to the concentration of 80% in complete medium,
631 they were then transfected with pEGFP-COX8 plasmid with lipofectamine 2000. After
632 24-48 h of transfection, G418 was added to screen positive monoclonal cells.

633 The lentiviral supernatant was prepared according to the protocol provided by
634 addgene (http://www.addgene.org/tools/protocols/plko/#A). When the confluence of
635 HEK293T cells cells in the 6-well plate reached 80%, Lipofectamine 2000 was used to
636 transfect the pLVX-mCherry-ACTIN plasmid and the viral packaging helper plasmid
637 psPAX2, pMD.2G into the cells. After incubation for 8h, the medium was replaced with
638 the fresh medium containing serum, and the supernatant was collected 24 hours and 48
639 hours later. The virus supernatant was filtered through a 0.45 μm pore so as to infect
640 COX8-EGFP-HeLa cells. Next, the COX8-EGFP-HeLa cells were cultured in a 6-well
641 plate to 70% confluence, then the medium was removed, and the virus supernatant was
642 mixed with fresh medium containing 8 μg/ml polybrene in equal proportions and added

643 to the culture plate. The fresh medium was replaced after 24 hours and the medium
644 containing 1 μg/ml puromycin was changed at 48 hours to start screening to obtain
645 stable cell lines.

646 **Cell Culture, Synchronization and Gamma irradiation**

647 HeLa, HEK-293T cell lines were purchased from American Type Cultures
648 Collection (ATCC, Manassas, VA). The HeLa and HEK-293T cells were cultured in
649 Dulbecco's modified Eagle's medium (DMEM, HyClone) containing 10% fetal bovine
650 serum (FBS, Gibco BRL). All cells were maintained at 37 °C in 5% CO2.

651 The cell cycle synchronization method was detailed in the previous
652 works(Rodríguez-Martínez et al., 2020). The cells were incubated with thymidine (2.5 mM)
653 for 18 hours, washed once with PBS buffer and replaced with fresh medium for 14
654 hours, and then 2.5 mM thymidine was added again to the cells which were then
655 incubated for 18 hours. The efficiency of synchronization was tested by flow cytometry
656 using cell cycle analysis kit (Multisciences).

657 HeLa cells were gamma-ray irradiated with a Biobeam Cs137 irradiator (cat no.
658 GM 2000; Gamma-Service Medical, Leipzig, Germany) at 1, 2, and 4 Gy witho the
659 dose rate of 3.37 Gy/min. In the control group, the cells were taken out of the incubator
660 without irradiation.

661 **Cell viablity, LDH measurements and colony-formation assays**

662 Cell viability was measured with CCK-8 assay kit (Dojindo, Japan). Briefly, 24 h
663 prior to irradiation treatment, ca. 6000 cells were plated in 96-well plates in a final
664 volume of 100 μl, and then cultured for 24h. And after adding the CCK-8 solution, the
665 plate was incubated for another 1 h. The optical density was measured at 450 nm using
666 a microplate reader (SpectraMax M5, Molecular Devices, USA). The amount of LDH
667 released into the medium was assayed using the LDH-Cytotoxicity Assay Kit II
668 (Dojindo, Japan) according to the manufacturer's instructions. For the colony formation
669 assay, 500 cells were seeded in 6-well plate. After being irradiated, the cells were
670 cultured at 37℃ for about 2 weeks. After carefully washing twice with PBS, 4%
671 paraformaldehyde was added to fix the cells. The the cells were then stained with crystal
672 violet solution and evaluated.

673 **Analysis of mitochondrial membrane potential and ROS**

674 TMRE-Mitochondrial membrane potential (MMP) assay kit (Useverbright, USA)
675 was used to measure MMP. The cells were incubated with culture medium containing
676 200 nM TMRE for 45 minutes at 37 °C, then rinsed with PBS 3 times, followed by
677 incubation with medium containing 50 nM TMRE. For the quantitative assessment, the
678 TMRE staining was evaluated using SpectraMax M5 microplate reader.

679 Reactive oxygen species (ROS) measurement was performed using H2DCFDA
680 (Sigma-Aldrich, USA) probe. 4×10^3 cells were seeded into 96-well plates and
681 incubated overnight. Before irradiation, the cells were incubated with HBSS solution

682 containing 5 μM H_2DCFDA for 15 minutes and then irradiated. After 30 minutes, the
683 cells were washed 3 times, followed by the fluorescence measurement using a
684 microtiter plate reader.

685 **Annexin V-FITC/PI staining and cell cycle analysis**

686 The HeLa cells were seeded at 2×10^5 cell /well in 6-well plates and irradiation
687 with gamma-ray. After 24 h, the cells were fixed with cold ethanol and then stained with
688 propidium iodide. The cells (about 20,000) were analyzed by flow cytometry (Beckman
689 CytoFLEX, USA). The total cells were washed once and resuspended in Annexin V
690 binding buffer, and then stained with 5 μl Annexin V and 5μl PI (Roche, Germany) for
691 20 min and analyzed with Beckman CytoFLEX flow cytometry. Ten thousand events
692 were collected for each sample.

693 **Measurement of mtDNA copy number**

694 Total genomic DNA of HeLa cells was extracted after irradiation using Total
695 genomic DNA extract kit (TAKARA, China). Human nuclear GAPDH gene (forward:
696 5′- CAGAACATCATCCCTGCCTCTAC-3′; reverse: 5′-
697 AAGGGTTGTAGTAGCCCGTAG-3′) and the mtDNA ND1 gene (forward: 5′-
698 TTCTAATCGCAATGGCATTCCT-3′; reverse: 5′-
699 AAGGGTTGTAGTAGCCCGTAG-3′), as well as a primer were used to detect the
700 mtDNA copy number. The real-time quantitative PCR analysis was performed using
701 SYBR Premix Ex Taq II (TAKARA, China) on LightCycler 480 PCR System (Roche,

Germany). The calculations were analyzed with $2^{-\Delta\Delta Ct}$ method.

Analysis of mean fluorescence intensity（MFI）of dual fluorescent protein

First, MFI of the dual fluorescent protein was analyzed using a flow cytometer. The cells were treated with different radiation doses and collected at different time points, washed once with PBS buffer, then assessed by flow cytometry (Beckman CytoFLEX, USA). The data were analyzed using Flow Jo software. The ratio of the MFI of EGFP to MFI of mecherry was used for calculation and analysis. Each irradiated dose sample group was analyzed for 10,000 cells, and three dishes were repeated.

Furthermore, the High-Content Screening system Cell Insight CX5 HCS (Thermo Fisher, Waltham, MA) was used for automatic photo quantitative analysis(Sun *et al,* 2016). The dual-fluorescent protein HeLa cells were seeded in 96-well plates by irradiated 1 Gy, 2 Gy, 4 Gy gamma ray. The nuclei were stained with Hoechst 33342 (Invitrogen, H3570). Fluorescence ratios of protein expression of mitochondrial expressed COX8-EGFP and actin-mCherry were statistically analyzed by cellomics software (Thermo Fisher, Waltham, MA).

Laser scanning confocal fluorescence microscopy

All the images were obtained using 488 nm and 561 nm lasers to excite cox8-EGFP-actin-mCherry, and 405 nm laser lines were used to excite DAPI. The imaging was performed in line mode, the z-stack was over-sampled and photographed at the height of 0.7 microns, and the image was acquired on the LEICA SP8 confocal

722 microscope system. The contrast and brightness of the image were adjusted by
723 Application Suite X (LEICA).

724 **Western blot analysis and immunofluorescence staining**

725 Total proteins were extracted from cells using RIPA lysis buffer with a protease
726 inhibitor cocktail (Roche, Germany). The proteins were quantified using Thermo
727 Scientific Pierce BCA Protein Assay. The protein level of Bax, Bcl-2, caspase-3,
728 cleaved caspase-9, Cytoc, PARP, TFAM, Mfn1, PGC-1α, GFP and loading control β-
729 Actin were determined by Western blot assay.

730 For immunofluorescence staining, HeLa cells were grown on chamber slides. After
731 γ-ray irradiation or mock irradiation, they were fixed with cold methanol for 10 minutes
732 and permeated with 0.5% Triton X-100 in PBS for 20 minutes. After blocking for 1
733 hour, the cells were incubated with the primary antibody overnight and then incubated
734 with the fluorescently labeled secondary antibody for 1 hour at 37°C. Samples
735 investigated by laser confocal microscopy (LEICA). Image auto-quantification and co-
736 localized foci were recognized by CellProfiler version 4
737 (www.cellprofiler.org)(McQuin *et al*, 2018).

738 **Statistical analysis**

739 Data were presented as mean ± standard deviation (SD). Statistical significance was
740 assessed by one-way or two-way ANOVA via GraphPad Prism software (Prism version
741 8, San Diego, CA, USA). *P*-Value < 0.05 was considered as statistically significant.

Data availability

This study includes no data deposited in external repositories.

Acknowledgments

This work was supported by the National Natural Science Foundation of China (grants No. 11635013 and No. 11775272) and Special Repair and Purchase Fund for Central-level scientific institutions (No. Y79XG13361).

Author contributions

QH conceived the idea and supervised the research. CS and QH designed and performed the experiments, analyzed and interpreted data, performed statistical analysis, and wrote the manuscript. XZ, YM, PW and QZ provided technical assistance in the experiments. All authors read and approved the final manuscript.

Competing interests

The authors declare that they have no competing interests.

Supplementary Information

Table S1

Oligonucleotides for amplify PCR product of COX8

Oligonucleotides	Sequence 5′ → 3′	size (bp)
Oligo1	CTAGAGATCTGGTACCGTCGACTGCAG AGATCCGCTAGGGGTACTCCGTG CCATCATGTCCGTCCTGACGCCGC TGCTGCTGCGGGGCTTGACAGGC TCGGCCCGGCGGCTCCCAGTGCC GCGCGCCAAGATCCATTCGTTGC CGCCGGAGGGG	154
Oligo2	AGCTTCCCCTCCGGCGGCAACGAATGG ATCTTGGCGCGCGGCACTGGGAG CCGCCGGGCCGAGCCTGTCAAGC CCCGCAGCAGCAGCGGCGTCAG GACGGACATGATGGCACGGAGTA CCCCTAGCGGATCTCTGCAGTCGA CGGTACCAGATCT	155

Expanded View Figures

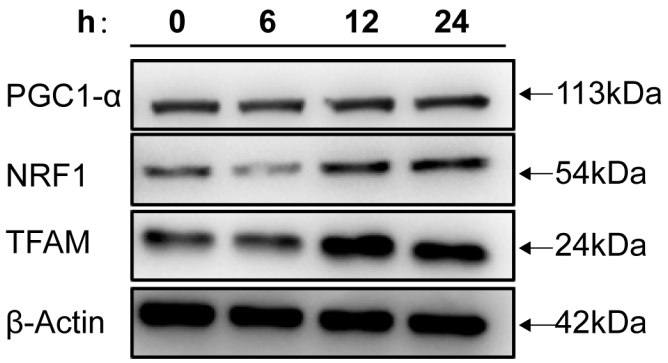

Figure EV1. Western blot assay for verifying the effect of AICAR on mitochondrial biogenesis.

HeLa cells were treated with mitochondrial biogenesis inducer drug (AICAR, 0.5 mM), and the whole cell extracts were collected at different time points. The mitochondrial biogenesis marker proteins (PGC-1α, NRF1 and TFAM) are indicated in the plot.

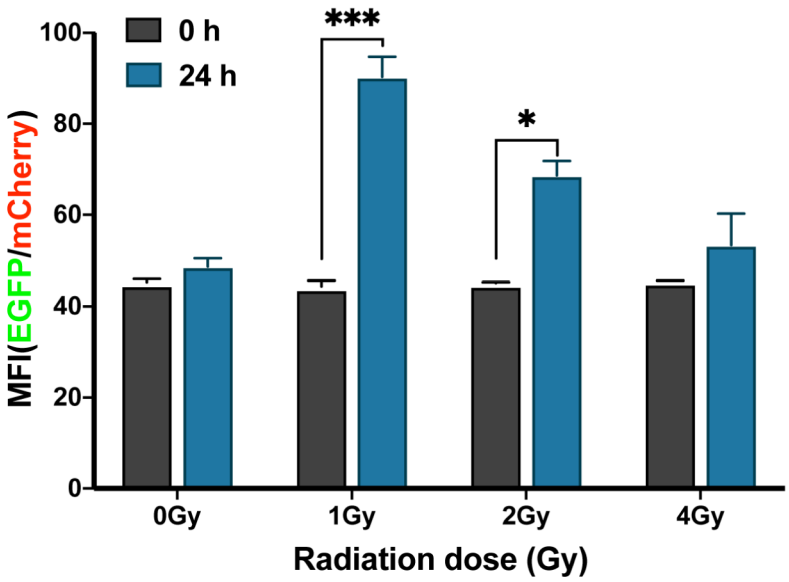

Figure EV2. The mean fluorescence intensity (MFI) of HeLa cells was determined by flow cytometry.

HeLa-cox8-EGFP-actin-mCherry cells were exposed to 1 Gy，2 Gy，4 Gy gamma-ray and incubated for the indicated periods. The analysis and comparison MFI obtained from the dual-fluorescent measurements by flow cytometry.

S1 Video

S2 Video

S3 Video

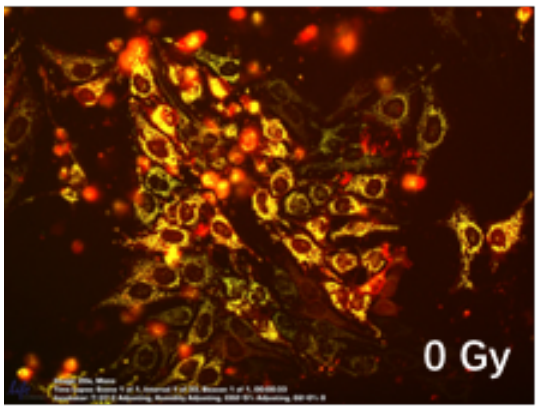

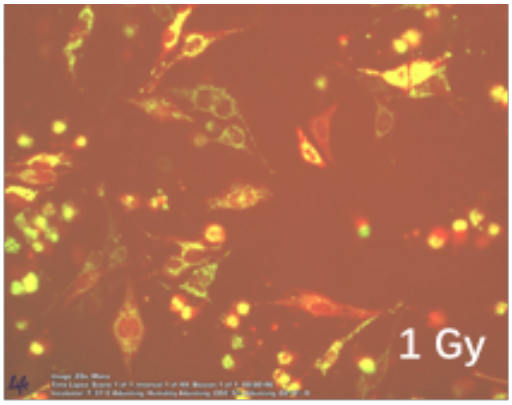

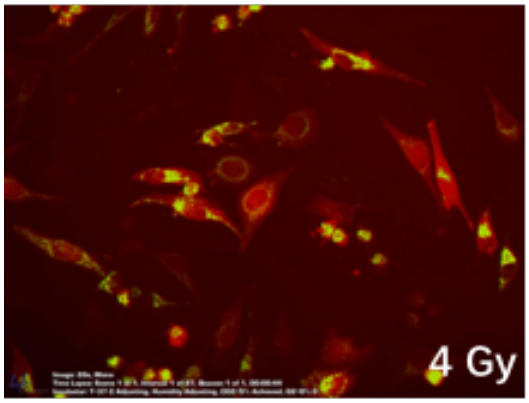

In-situ real-time video of dual fluorescence reporter system of irradiated cells (Video S1, Video S2, Video S3)

References:

Azzam EI, Jay-Gerin J-P & Pain D (2012) Ionizing radiation-induced metabolic oxidative stress and prolonged cell injury. *Cancer Lett* 327: 48–60

Barros MH & McStay GP (2019) Modular Biogenesis of Mitochondrial Respiratory Complexes. *Mitochondrion* 50: 94–114

Bernstein C, Bernstein H, Payne CM & Garewal H (2002) DNA repair/pro-apoptotic dual-role proteins in five major DNA repair pathways: fail-safe protection against carcinogenesis. *Mutat Res Rev Mutat Res* 511: 145–178

800 Betzig E, Patterson GH, Sougrat R, Lindwasser OW, Olenych S, Bonifacino JS, Davidson MW,
801 Lippincott-Schwartz J & Hess HF (2006) Imaging Intracellular Fluorescent Proteins at
802 Nanometer Resolution. *Science* 313: 1642–1645

803 Burke PJ (2017) Mitochondria, Bioenergetics and Apoptosis in Cancer. *Trends Cancer* 3: 857–
804 870

805 Cao C, Yu H, Wu F, Qi H & He J (2017) Antibiotic anisomycin induces cell cycle arrest and
806 apoptosis through inhibiting mitochondrial biogenesis in osteosarcoma. *J Bioenerg Biomembr*
807 49: 437–443

808 Chalkiadaki A & Guarente L (2015) The multifaceted functions of sirtuins in cancer. *Nat Rev*
809 *Cancer* 15: 608–624

810 Dam AD, Mitchell AS & Quadrilatero J (2013) Induction of mitochondrial biogenesis protects
811 against caspase-dependent and caspase-independent apoptosis in L6 myoblasts. *Biochimica Et*
812 *Biophysica Acta Bba - Mol Cell Res* 1833: 3426–3435

813 Das S, Joshi MB, Parashiva GK & Rao SBS (2020) Stimulation of cytoprotective autophagy and
814 components of mitochondrial biogenesis / proteostasis in response to ionizing radiation as a
815 credible pro-survival strategy. *Free Radical Bio Med*

816 Davis AJ, Chen BPC & Chen DJ (2014) DNA-PK: A dynamic enzyme in a versatile DSB repair
817 pathway. *Dna Repair* 17: 21–29

818 Fanibunda SE, Deb S, Maniyadath B, Tiwari P, Ghai U, Gupta S, Figueiredo D, Weisstaub N,
819 Gingrich JA, Vaidya ADB, *et al* (2019) Serotonin regulates mitochondrial biogenesis and
820 function in rodent cortical neurons via the 5-HT2A receptor and SIRT1–PGC-1α axis. *Proc*
821 *National Acad Sci* 116: 201821332

822 Fu X, Wan S, Lyu YL, Liu LF & Qi H (2008) Etoposide Induces ATM-Dependent Mitochondrial
823 Biogenesis through AMPK Activation. *Plos One* 3: e2009

824 Galluzzi L & Kroemer G (2008) Necroptosis: a specialized pathway of programmed necrosis. *Cell*
825 135: 1161–3

826 Haggie PM & Verkman AS (2002) Diffusion of Tricarboxylic Acid Cycle Enzymes in the
827 Mitochondrial Matrixin Vivo: EVIDENCE FOR RESTRICTED MOBILITY OF A
828 MULTIENZYME COMPLEX. *J Biol Chem* 277: 40782–40788

829 Hanson GT, Aggeler R, Oglesbee D, Cannon M, Capaldi RA, Tsien RY & Remington SJ (2004)
830 Investigating Mitochondrial Redox Potential with Redox-sensitive Green Fluorescent Protein
831 Indicators. *J Biol Chem* 279: 13044–13053

832 Holler N, Zaru R, Micheau O, Thome M, Attinger A, Valitutti S, Bodmer J-L, Schneider P, Seed
833 B & Tschopp J (2000) Fas triggers an alternative, caspase-8–independent cell death pathway
834 using the kinase RIP as effector molecule. *Nat Immunol* 1: 489–495

835 Huangyang P, Li F, Lee P, Nissim I, Weljie AM, Mancuso A, Li B, Keith B, Yoon SS & Simon
836 MC (2020) Fructose-1,6-Bisphosphatase 2 Inhibits Sarcoma Progression by Restraining
837 Mitochondrial Biogenesis. *Cell Metab* 31: 1032

838 Jadhav U & Shivdasani RA (2019) Dissecting Cell Lineages: From Microscope to Kaleidoscope.
839 *Cell* 176: 949–951

840 Katajisto P, Döhla J, Chaffer CL, Pentinmikko N, Marjanovic N, Iqbal S, Zoncu R, Chen W,
841 Weinberg RA & Sabatini DM (2015) Stem cells. Asymmetric apportioning of aged
842 mitochondria between daughter cells is required for stemness. *Sci New York N Y* 348: 340–3

843 Kim J, Yang G, Kim Y, Kim J & Ha J (2016) AMPK activators: mechanisms of action and
844 physiological activities. *Exp Mol Medicine* 48: e224–e224

845 Kluza J, Marchetti P, Gallego M-A, Lancel S, Fournier C, Loyens A, Beauvillain J-C & Bailly C
846 (2004) Mitochondrial proliferation during apoptosis induced by anticancer agents: effects of
847 doxorubicin and mitoxantrone on cancer and cardiac cells. *Oncogene* 23: 7018–7030

848 Komen JC & Thorburn DR (2014) Turn up the power – pharmacological activation of
849 mitochondrial biogenesis in mouse models. *Brit J Pharmacol* 171: 1818–1836

850 Kulms D, Zeise E, Pöppelmann B & Schwarz T (2002) DNA damage, death receptor activation
851 and reactive oxygen species contribute to ultraviolet radiation-induced apoptosis in an
852 essential and independent way. *Oncogene* 21: 5844–5851

853 Leach JK, Tuyle GV, Lin PS, Schmidt-Ullrich R & Mikkelsen RB (2001) Ionizing radiation-
854 induced, mitochondria-dependent generation of reactive oxygen/nitrogen. *Cancer Res* 61:
855 3894–901

856 Lee H-C & Wei Y-H (2005) Mitochondrial biogenesis and mitochondrial DNA maintenance of
857 mammalian cells under oxidative stress. *Int J Biochem Cell Biology* 37: 822–834

858 Li S, Shi B, Liu X & An H-X (2020) Acetylation and Deacetylation of DNA Repair Proteins in
859 Cancers. *Frontiers Oncol* 10: 573502

860 Lill R & Freibert S-A (2020) Mechanisms of Mitochondrial Iron-Sulfur Protein Biogenesis. *Annu*
861 *Rev Biochem* 89: 471–499

862 Lin WT, Nithiyanantham S, Hsieh DJ, Chen R, Day C, Liao JY, Kuo C, Mahalakshmi B, Kuo W
863 & Huang C (2020) Bioactive peptides attenuate cardiac apoptosis in spontaneously
864 hypertensive rat hearts through activation of autophagy and mitochondrial biogenesis pathway.
865 *Environ Toxicol* 35: 804–810

866 Llopis J, McCaffery JM, Miyawaki A, Farquhar MG & Tsien RY (1998) Measurement of
867 cytosolic, mitochondrial, and Golgi pH in single living cells with green fluorescent proteins.
868 *Proc National Acad Sci* 95: 6803–6808

869 Löbrich M & Jeggo PA (2005) Harmonising the response to DSBs: a new string in the ATM bow.
870 *Dna Repair* 4: 749–759

871 Luo C, Widlund HR & Puigserver P (2016) PGC-1 Coactivators: Shepherding the Mitochondrial
872 Biogenesis of Tumors. *Trends Cancer* 2: 619–631

873 Mahajan NP, Linder K, Berry G, Gordon GW, Heim R & Herman B (1998) Bcl-2 and Bax
874 interactions in mitochondria probed with green fluorescent protein and fluorescence resonance
875 energy transfer. *Nat Biotechnol* 16: 547–552

876 Martins LAM, Vieira MQ, Ilha M, Vasconcelos M de, Biehl HB, Lima DB, Schein V, Barbé-
877 Tuana F, Borojevic R & Guma FCR (2015) The Interplay Between Apoptosis, Mitophagy and
878 Mitochondrial Biogenesis Induced by Resveratrol Can Determine Activated Hepatic Stellate
879 Cells Death or Survival. *Cell Biochem Biophys* 71: 657–672

880 May-Panloup P, Vignon X, Chrétien M-F, Heyman Y, Tamassia M, Malthièry Y & Reynier P
881 (2005) Increase of mitochondrial DNA content and transcripts in early bovine embryogenesis
882 associated with upregulation of mtTFA and NRF1 transcription factors. *Reprod Biol Endocrin*
883 3: 65

884 McQuin C, Goodman A, Chernyshev V, Kamentsky L, Cimini BA, Karhohs KW, Doan M, Ding
885 L, Rafelski SM, Thirstrup D, *et al* (2018) CellProfiler 3.0: Next-generation image processing
886 for biology. *Plos Biol* 16: e2005970

887 Melentijevic I, Toth ML, Arnold ML, Guasp RJ, Harinath G, Nguyen KC, Taub D, Parker JA,
888 Neri C, Gabel CV, *et al* (2017) C. elegans neurons jettison protein aggregates and
889 mitochondria under neurotoxic stress. *Nature* 542: 367–371

890 Mihaylova MM & Shaw RJ (2011) The AMPK signalling pathway coordinates cell growth,
891 autophagy and metabolism. *Nat Cell Biol* 13: 1016–1023

892 Miyashiro T & Goulian M (2007) Methods in Enzymology. *Methods Enzymol* 423: 458–475

893 Mukhopadhyay P, Rajesh M, Haskó G, Hawkins BJ, Madesh M & Pacher P (2007) Simultaneous
894 detection of apoptosis and mitochondrial superoxide production in live cells by flow cytometry
895 and confocal microscopy. *Nat Protoc* 2: 2295–2301

896 Newman RH, Fosbrink MD & Zhang J (2011) Genetically encodable fluorescent biosensors for
897 tracking signaling dynamics in living cells. *Chem Rev* 111: 3614–66

898 O'Driscoll M & Jeggo PA (2006) The role of double-strand break repair — insights from human
899 genetics. *Nat Rev Genet* 7: 45–54

900 Paredes S & Chua KF (2016) SIRT7 clears the way for DNA repair. *Embo J* 35: 1483–1485

901 Park S-J, Gavrilova O, Brown AL, Soto JE, Bremner S, Kim J, Xu X, Yang S, Um J-H, Koch LG,
902 *et al* (2017) DNA-PK Promotes the Mitochondrial, Metabolic, and Physical Decline that
903 Occurs During Aging. *Cell Metab* 25: 1135-1146.e7

904 Popov L (2020) Mitochondrial biogenesis: An update. *J Cell Mol Med* 24: 4892–4899

905 Rai PK, Russell OM, Lightowlers RN & Turnbull DM (2015) Potential compounds for the
906 treatment of mitochondrial disease. *Brit Med Bull* 116: 5–18

907 Rai Y, Pathak R, Kumari N, Sah DK, Pandey S, Kalra N, Soni R, Dwarakanath BS & Bhatt AN
908 (2018) Mitochondrial biogenesis and metabolic hyperactivation limits the application of MTT
909 assay in the estimation of radiation induced growth inhibition. *Sci Rep-uk* 8: 1531

910 Ruan L, Zhou C, Jin E, Kucharavy A, Zhang Y, Wen Z, Florens L & Li R (2017) Cytosolic
911 proteostasis through importing of misfolded proteins into mitochondria. *Nature* 543: 443–446

912 Scarpulla RC (2008) Transcriptional Paradigms in Mammalian Mitochondrial Biogenesis and
913 Function. *Physiol Rev* 88: 611–638

914 Spitz DR, Azzam EI, Li JJ & Gius D (2004) Metabolic oxidation/reduction reactions and cellular
915 responses to ionizing radiation: A unifying concept in stress response biology. *Cancer Metast*
916 *Rev* 23: 311–322

917 Srinivas US, Tan BWQ, Vellayappan BA & Jeyasekharan AD (2019) ROS and the DNA damage
918 response in cancer. *Redox Biol* 25: 101084

919 Sun J, Li N, Oh K-S, Dutta B, Vayttaden SJ, Lin B, Ebert TS, Nardo DD, Davis J, Bagirzadeh R,
920 *et al* (2016) Comprehensive RNAi-based screening of human and mouse TLR pathways
921 identifies species-specific preferences in signaling protein use. *Sci Signal* 9: ra3–ra3

922 Vayssiere JL, Petit PX, Risler Y & Mignotte B (1994) Commitment to apoptosis is associated
923 with changes in mitochondrial biogenesis and activity in cell lines conditionally immortalized
924 with simian virus 40. *Proc National Acad Sci* 91: 11752–11756

925 Virbasius CA, Virbasius JV & Scarpulla RC (1993) NRF-1, an activator involved in nuclear-
926 mitochondrial interactions, utilizes a new DNA-binding domain conserved in a family of
927 developmental regulators. *Gene Dev* 7: 2431–2445

928 Vyas S, Zaganjor E & Haigis MC (2016) Mitochondria and Cancer. *Cell* 166: 555–566

929 Westermann B & Neupert W (2000) Mitochondria-targeted green fluorescent proteins: convenient
930 tools for the study of organelle biogenesis inSaccharomyces cerevisiae. *Yeast* 16: 1421–1427

931 Wu Z, Puigserver P, Andersson U, Zhang C, Adelmant G, Mootha V, Troy A, Cinti S, Lowell B,
932 Scarpulla RC, *et al* (1999) Mechanisms Controlling Mitochondrial Biogenesis and Respiration
933 through the Thermogenic Coactivator PGC-1. *Cell* 98: 115–124

934 Yambire KF, Fernandez-Mosquera L, Steinfeld R, Mühle C, Ikonen E, Milosevic I & Raimundo
935 N (2019) Mitochondrial biogenesis is transcriptionally repressed in lysosomal lipid storage
936 diseases. *Elife* 8: e39598

937 Yu H, Zhao W, Xie M, Li X, Sun M, He J, Wang L & Yu L (2020) Real-Time Monitoring of Self-
938 Aggregation of β-Amyloid by a Fluorescent Probe Based on Ruthenium Complex. *Anal Chem*
939 92: 2953–2960

940 Yu J, Wang Q, Chen N, Sun Y, Wang X, Wu L, Chen S, Yuan H, Xu A & Wang J (2013)
941 Mitochondrial transcription factor A regulated ionizing radiation-induced mitochondrial
942 biogenesis in human lung adenocarcinoma A549 cells. *J Radiat Res* 54: 998–1004

943 Yu M (2011) Generation, function and diagnostic value of mitochondrial DNA copy number
944 alterations in human cancers. *Life Sci* 89: 65–71

945 Zhang T, Ikejima T, Li L, Wu R, Yuan X, Zhao J, Wang Y & Peng S (2017) Impairment of
946 Mitochondrial Biogenesis and Dynamics Involved in Isoniazid-Induced Apoptosis of HepG2
947 Cells Was Alleviated by p38 MAPK Pathway. *Front Pharmacol* 8: 753

948